Mathematical Biosciences 368 (2024) 109133

Contents lists available at ScienceDirect

Mathematical Biosciences

journal homepage: www.elsevier.com/locate/mbs

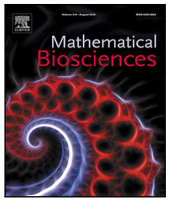

Original Research Article

Modeling the impact of hospital beds and vaccination on the dynamics of an infectious disease

Jyoti Maurya [a], Konstantin B. Blyuss [b], A.K. Misra [a,*]

[a] Department of Mathematics, Institute of Science, Banaras Hindu University, Varanasi 221 005, India
[b] Department of Mathematics, University of Sussex, Falmer, Brighton, BN1 9QH, United Kingdom

ARTICLE INFO

Keywords:
Hospital beds
Vaccination
Bifurcations

ABSTRACT

The unprecedented scale and rapidity of dissemination of re-emerging and emerging infectious diseases impose new challenges for regulators and health authorities. To curb the dispersal of such diseases, proper management of healthcare facilities and vaccines are core drivers. In the present work, we assess the unified impact of healthcare facilities and vaccination on the control of an infectious disease by formulating a mathematical model. To formulate the model for any region, we consider four classes of human population; namely, susceptible, infected, hospitalized, and vaccinated. It is assumed that the increment in number of beds in hospitals is continuously made in proportion to the number of infected individuals. To ensure the occurrence of transcritical, saddle–node and Hopf bifurcations, the conditions are derived. The normal form is obtained to show the existence of Bogdanov–Takens bifurcation. To validate the analytically obtained results, we have conducted some numerical simulations. These results will be useful to public health authorities for planning appropriate health care resources and vaccination programs to diminish prevalence of infectious diseases.

1. Introduction

In the pre-modern era, the global spread of infectious diseases caused high mortality and morbidity with devastating consequences. However, medical advances, improved access to healthcare, and the development of vaccines have contributed to a decline in overall mortality and morbidity linked to infectious diseases [1]. Nevertheless the burden of death linked with infectious diseases remains substantial in lower- and middle-income countries [2]. The ability to minimize the impact of these possible disease threats depends on appropriate healthcare services including number of hospital beds. It is impossible to give a one-size-fits-all answer to the question of how many hospital beds a country should have per 10,000 people, as it depends on a variety of factors, such as immunity, fooding habits and environment of that particular region. However, the World Health Organization (WHO) provides guidance that this Hospital-beds-population-ratio (HBPR) should lie between 21 to 165 [3]. By way of example, for Asian countries, HBPR, per 10,000 inhabitants and mortality linked to infectious diseases (for year 2019), per 10,000 inhabitants is shown in Fig. 1. Concatenating the aforementioned data, we observe that the countries with HBPR 29 and higher have low mortality, whereas countries with HBPR under 10 experienced a high rate of mortality linked to infectious diseases, Fig. 2. Although mortality related to infectious diseases also depends on some other factors (such as lifestyle and seasonal fluctuations) and circumstances, HBPR nevertheless is a core driver to control of their prevalence.

As we say "prevention is always better than cure", the vaccine has been proved to be the strongest footprint in this regard as it has shown positive results in fighting against infectious diseases [5]. It would be impossible to predict the effects of vaccines in a counterfactual world in which vaccines had not been developed. For example, smallpox was once a widespread and deadly disease, but vaccination against it in 1977 is a monumental leap, that rooted out the disease completely. From the history of polio and smallpox to the present day of COVID-19, vaccines have been proven as the savviest way to tackle the deadliest diseases and have been the shining hope whenever diseases have almost devastated economies and people's life. Vaccines have the potential to root out infectious diseases locally without global eradication and along with the proper management of healthcare facilities are milestones for public health interventions.

The relationship between healthcare and vaccines is bidirectional, as healthcare impacts the dynamics of infectious diseases in the early stage of their encounter, while vaccines include long-term goals. In this regard, some mathematical modelers have put their efforts to study the impact of healthcare facilities or vaccination on disease dynamics [6–24]. In particular, Abdelrazec et al. [6] proposed a deterministic model

* Corresponding author.
E-mail address: akmisra_knp@yahoo.com (A.K. Misra).

https://doi.org/10.1016/j.mbs.2023.109133
Received 27 April 2023; Received in revised form 26 October 2023; Accepted 19 December 2023
Available online 23 December 2023

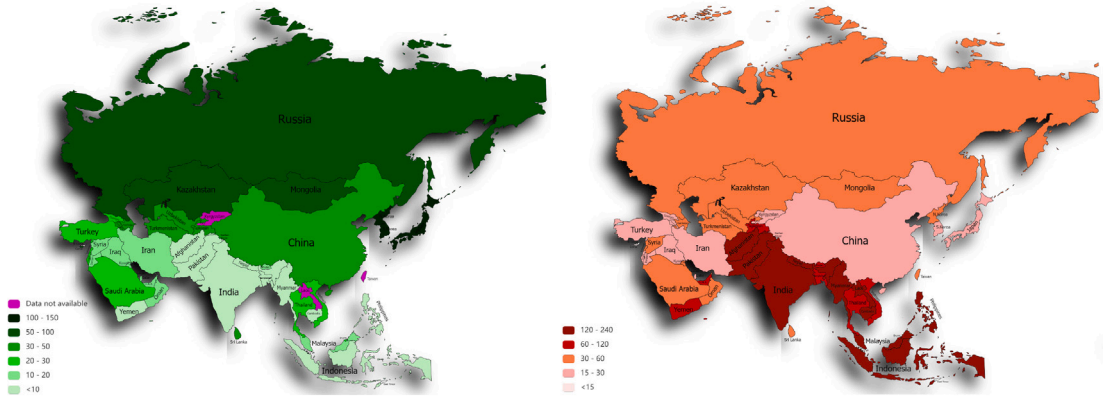

Fig. 1. (a) HBPR of Asian countries, per 10,000 people (most recent data available at [4]) (b) Number of deaths in Asian countries due to infectious diseases, per 10,00,000 people [2].

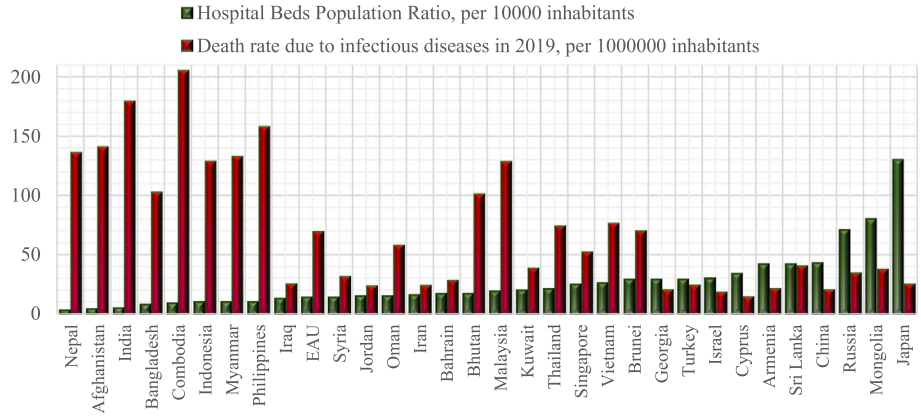

Fig. 2. Bar plot for HBPR per 10,000 and number of deaths in Asian countries due to infectious diseases, per 1000000 people [2,4].

for the study of dengue fever transmission dynamics as well as the impact of available healthcare resources on the spread and control of disease. They concluded that only the basic reproduction number is not enough for the understanding of disease transmission dynamics, other epidemiological parameters, such as HBPR also drastically affects disease transmission dynamics. Zhou and Fan [25] have studied an SIR epidemic model to show the impact of limited medical resources on the transmission dynamics of infectious diseases. According to their study, the availability and supply efficiency of medical resources have a powerful impact on the control of infectious diseases. Arino and Milliken [26] studied the effect of vaccination on the disease prevalence, by adding a compartment for vaccinated individuals to their SLIARS (susceptible-latent-infected-asymptotic-recovered-susceptible) model and contemplating disease-induced death, waning infection-acquired immunity, and imperfect and waning vaccination protection.

The normal questions asked by people in the midst of an epidemic outbreak are: Can the diseases be rooted out or persist? If the disease persists, how will the healthcare facilities be managed? How will vaccination programs be implemented effectively? To answer all these questions and study the unified effect of healthcare facilities (in terms of hospital beds) and vaccines on infectious disease dynamics, we devise a mathematical model. Additionally, we consider that the number of hospital beds is made continuously proportional to the number of infected individuals.

2. The mathematical model

For the region under consideration, we divide the total human population into four sub-populations: susceptible (S), infected (I), hospitalized (H) and vaccinated (V). We consider that recruitment of individuals in susceptible class occurs at a rate A. In the absence of vaccines and healthcare facilities (more precisely, the number of hospital beds), there is a probability that some susceptible individuals may acquire the infection when they get in physical touch with infected individuals. This transmission of individuals from S class to I class occurs at a rate β. The disease-induced mortality is represented by α. Also, some infected individuals recover on their own and join the susceptible class, with a self-recovery rate ν. The parameter d, represents natural mortality. The time evolution of the infectious disease can be modeled mathematically with the help of following system of non-linear differential equations.

$$\begin{cases} \dfrac{dS}{dt} = A - \beta SI - dS + \nu I, \\ \dfrac{dI}{dt} = \beta SI - (\nu + \alpha + d)I. \end{cases} \tag{1}$$

To study the impact of hospital beds and vaccination, we introduce two new dynamical variables for human population $H(t)$ and $V(t)$, that represent hospitalized and vaccinated individuals, respectively at time $t \geq 0$. The sudden increase in the infected population increases the congregation in hospitals. To fulfill this demand, an increase in hospital beds is necessary. Thus, we introduce a state variable H_b, representing the increment in hospital beds, that occurs at a rate ϕ proportional to the number of infected individuals. Due to some financial reservations and manufacturing errors, some newly created hospital beds do not contribute and thus decrease at a rate ϕ_0. The total number of pre-existing hospital beds is H_a. Thus, $(H_a + H_b - H)$ represents available number of hospital beds for the use of infected individuals at time

$t > 0$. Note that maximum $(H_a + H_b)$ individuals can be admitted to hospitals at any time t, therefore $(H_a + H_b - H) \geq 0$, and k_1 is the hospitalization rate coefficient. Furthermore, we assume vaccination of the susceptible population transpires at a rate σ. Due to some inefficacy of vaccination, a few vaccinated individuals may acquire infection and join the infected class with transmission rate β_1. The constant θ and ν_1 represent extra disease-induced mortality recovery rate of infected individuals in hospitals, respectively. Using these assumptions, model system (1) modifies to

$$\begin{cases} \dfrac{dS}{dt} = A - \beta SI - dS - \sigma S + \nu I + \nu_1 H, \\ \dfrac{dI}{dt} = \beta SI + \beta_1 VI - (\nu + \alpha + d)I - k_1(H_a + H_b - H)I, \\ \dfrac{dH}{dt} = k_1(H_a + H_b - H)I - (d + \theta\alpha + \nu_1)H, \\ \dfrac{dV}{dt} = \sigma S - dV - \beta_1 VI, \\ \dfrac{dH_b}{dt} = \phi I - \phi_0 H_b. \end{cases} \tag{2}$$

Here, $S(0) > 0$, $I(0) \geq 0$, $H(0) \geq 0$, $V(0) > 0$, and $H_b(0) \geq 0$. Also, all the considered parameters are non-negative.

3. Basic properties

3.1. Disease-free equilibrium and basic reproduction number

We can see that system (2) always exhibits a unique disease-free equilibrium $E_0\left(\frac{A}{d+\sigma}, 0, 0, \frac{\sigma A}{d(d+\sigma)}, 0\right)$. Now, we calculate the basic reproduction number for the proposed model system (2) using next-generation matrix method [27]. The transmission and transition matrices in the model system (2) are respectively given as

$$\mathcal{T}_F = \left[\beta SI + \beta_1 VI\right], \text{ and } \mathcal{T}_M = \left[(\nu + \alpha + d)I + k_1(H_a + H_b - H)I\right].$$

The transmission (new infection) and transition matrices at equilibrium E_0 are respectively

$$T_F = \begin{bmatrix} \frac{\beta A}{(d+\sigma)} + \frac{\beta_1 \sigma A}{d(d+\sigma)} \end{bmatrix}, \text{ and } T_M = \begin{bmatrix} \nu + \alpha + d + k_1 H_a \end{bmatrix}.$$

Thus,

$$T_F(T_M)^{-1} = \begin{bmatrix} \left(\frac{\beta A}{(d+\sigma)} + \frac{\beta_1 \sigma A}{d(d+\sigma)}\right) \times \left(\frac{1}{\nu+\alpha+d+k_1 H_a}\right) \end{bmatrix}.$$

As model system (2) has only one infected class, i.e., I; thus, the entry in matrix T_F indicates that the rate at which number of infected individuals are produced in class I, whereas the entry in T_M represents the expected time an individual spends in class I. Furthermore, the entry in $T_F(T_M)^{-1}$ is the expected number of secondary infection in class I produced by a typically infected individuals during his/ her whole infectious period in a totally susceptible population. Thus, the basic reproduction number for model system (2) can be written as

$$R_0 = \frac{\beta A}{(d+\sigma)(\nu+\alpha+d+k_1 H_a)} + \frac{\beta_1 A}{(d+\sigma)(\nu+\alpha+d+k_1 H_a)} \frac{\sigma}{d}.$$

3.2. Endemic equilibrium

Now, for any endemic equilibrium $E(S, I, H, V, H_b)$, the components S, H, V, and H_b can be expressed in terms of I as follows

$$S(I) = \frac{\phi_0(d + \theta\alpha + \nu_1 + k_1 I)(\nu + \alpha + d) + k_1\left((\phi_0 H_a + \phi I)(d + \theta\alpha + \nu_1)\right)}{\phi_0(d + \theta\alpha + \nu_1 + k_1 I)\left(\beta + \frac{\beta_1\sigma}{\beta_1 I + d}\right)},$$

$$H(I) = \frac{k_1(\phi_0 H_a + \phi I)I}{\phi_0(d + \theta\alpha + \nu_1 + k_1 I)},$$

$$V(I) = \frac{\sigma}{(d + \beta_1 I)} S(I), \text{ and } H_b(I) = \frac{\phi}{\phi_0} I.$$

Table 1
The case $R_0 > 1$.

Δ_0	$\mathcal{D}_2$	$\mathcal{D}_3$	Number of positive solutions of $\mathcal{P}(I) = 0$
$\Delta_0 > 0$	–	< 0	1
$\Delta_0 > 0$	> 0	> 0	1
$\Delta_0 > 0$	< 0	> 0	1 if $\mathcal{P}(I_-)\mathcal{P}(I_+) > 0$ 3 if $\mathcal{P}(I_-)\mathcal{P}(I_+) < 0$
$\Delta_0 < 0$	–	–	1

Table 2
The case $R_0 < 1$.

Δ_0	$\mathcal{D}_2$	$\mathcal{D}_3$	Number of positive solutions of $\mathcal{P}(I) = 0$
$\Delta_0 > 0$	–	< 0	0 if $\mathcal{P}(I_+) > 0$ 2 if $\mathcal{P}(I_+) < 0$
$\Delta_0 > 0$	< 0	> 0	0 if $\mathcal{P}(I_+) > 0$ 2 if $\mathcal{P}(I_+) < 0$
$\Delta_0 > 0$	> 0	> 0	0
$\Delta_0 < 0$	–	–	0

In the above expressions, the coordinate I is a positive root of the following cubic equation

$$\mathcal{P}(I) = \mathcal{D}_1 I^3 + \mathcal{D}_2 I^2 + \mathcal{D}_3 I + \mathcal{D}_4 = 0, \tag{3}$$

where

$$\begin{aligned}
\mathcal{D}_1 &= \beta\beta_1 k_1\left[\phi_0(\alpha + d) + \phi(d + \theta\alpha)\right], \\
\mathcal{D}_2 &= -\beta\beta_1\phi_0 k_1 A + \phi_0(\alpha + d)[k_1(\beta d + \beta_1\sigma) + \beta\beta_1(d + \theta\alpha + \nu_1)] \\
&\quad + k_1(d + \theta\alpha)[\beta\beta_1\phi_0 H_a + \phi(\beta d + \beta_1\sigma)] \\
&\quad + \beta_1\phi_0 k_1 d(\nu + \alpha + d + k_1 H_a) + \beta_1 k_1 d[\phi(d + \theta\alpha + \nu_1) - k_1\phi_0 H_a], \\
\mathcal{D}_3 &= -\phi_0 k_1 d(R_0 - 1)(d + \sigma)(\nu + \alpha + d + k_1 H_a) \\
&\quad - \beta\beta_1\phi_0 A(d + \theta\alpha + \nu_1) + dk_1(d + \sigma)[\phi(d + \theta\alpha + \nu_1) - k_1\phi_0 H_a] \\
&\quad + \phi_0(\alpha + d)(d + \theta\alpha + \nu_1)(\beta d + \beta_1\sigma) + \phi_0 H_a k_1(d + \theta\alpha)(\beta d + \beta_1\sigma) \\
&\quad + \beta\phi_0 d(d + \theta\alpha + \nu_1)(\nu + \alpha + d + k_1 H_a), \\
\mathcal{D}_4 &= -d\phi_0(R_0 - 1)(d + \sigma)(d + \theta\alpha + \nu_1)(\nu + \alpha + d + k_1 H_a).
\end{aligned}$$

From equation $\mathcal{P}(I) = 0$, we observe that $\mathcal{D}_1$ is always positive, and $\mathcal{D}_4 > 0$ if $R_0 < 1$, and $\mathcal{D}_4 < 0$ for $R_0 > 1$. Thus, to get a qualitative analysis of positive solutions of $\mathcal{P}(I) = 0$, we look at the derivative $(d\mathcal{P}/dI) = 3\mathcal{D}_1 I^2 + 2\mathcal{D}_2 I + \mathcal{D}_3$ and set $\Delta_0 = \mathcal{D}_2^2 - 3\mathcal{D}_1\mathcal{D}_3$. Then, we have two cases according to the value of R_0.

(i) When $R_0 > 1$.
In this case $\mathcal{D}_4 < 0$. Now, second degree polynomial $(d\mathcal{P}/dI)$ has two real solutions I_+ and I_- when $\Delta_0 > 0$, which determines the existence of one or three positive solutions of equation $\mathcal{P}(I) = 0$. Thus, we have two cases: (a) if $I_- < 0 < I_+$ or $I_- < I_+ < 0$, then equation $\mathcal{P}(I) = 0$ has one positive solution, and (b) if $0 < I_- < I_+$, then equation $\mathcal{P}(I)=0$ gives three positive solutions when $\mathcal{P}(I_-)\mathcal{P}(I_+) < 0$ and one positive solution otherwise. Also, when $\Delta_0 < 0$, the equation $\mathcal{P}(I) = 0$ gives one positive solution. These results are summarized in Table 1.

(ii) When $R_0 < 1$.
In this case $\mathcal{D}_4 > 0$. If $\Delta_0 > 0$, then second degree polynomial $d\mathcal{P}/dI$ has two solutions I_- and I_+, which determines the existence of zero or two positive solutions for the equation $\mathcal{P}(I) = 0$. Thus, we have two cases: (a) if $I_- < 0 < I_+$ or $0 < I_- < I_+$, then equation $\mathcal{P}(I) = 0$ has two positive solutions if $\mathcal{P}(I_+) < 0$ or no positive solution otherwise. (b) If $I_- < I_+ < 0$, then $\mathcal{P}(I) = 0$ will always return to no positive solution. These results are summarized in Table 2.

We also observe that if $D_3 < 0$, then $\triangle_0 > 0$. Thus, for $R_0 < 1$, the value of $\mathcal{P}(I_+) = 0$ gives a threshold value (R_0^*) of R_0 for saddle–node bifurcation. Thus, we establish the following theorem.

Theorem 1. *The system (2) may admits*

(i) Two endemic equilibria E_1^* (with high endemicity) and E_2^* (with low endemicity) when $R_0^* < R_0 < 1$, coalesce into E_3^* at $R_0 = R_0^*$, and ceases to appear when $R_0 < R_0^*$.

(ii) A unique endemic equilibrium E_1^* when $R_0 > 1$.

3.3. Stability analysis of obtained equilibria

3.3.1. Disease-free equilibrium

The Jacobian matrix for model system (2) computed at $E_0\left(\frac{A}{d+\sigma}, 0, 0, \frac{\sigma A}{d(d+\sigma)}, 0\right)$ is given by

$$J_0 = \begin{bmatrix} -(d+\sigma) & -\beta\left(\frac{A}{d+\sigma}\right)+\nu & \nu_1 & 0 & 0 \\ 0 & (R_0-1)(\nu+\alpha+d+k_1H_a) & 0 & 0 & 0 \\ 0 & k_1H_a & -(d+\theta\alpha+\nu_1) & 0 & 0 \\ \sigma & -\frac{\beta_1\sigma A}{d(d+\sigma)} & 0 & -d & 0 \\ 0 & \phi & 0 & 0 & -\phi_0 \end{bmatrix}.$$

The eigenvalues of above matrix are

$$-(d+\sigma),\quad (R_0-1)(\nu+\alpha+d+k_1H_a),\quad -(d+\theta\alpha+\nu_1),\quad -d,\quad -\phi_0.$$

Here, the four eigenvalues of matrix J_0 are always negative and the second eigenvalue is negative for $R_0 < 1$ and positive for $R_0 > 1$. Thus, we establish the following theorem.

Theorem 2. *The equilibrium E_0 is locally asymptotically stable for $R_0 < 1$ and unstable for $R_0 > 1$.*

3.3.2. Endemic equilibrium

The Jacobian matrix for model system (2) evaluated at endemic equilibrium E (either E_1^* or E_2^*) is given by

$$J^* = \begin{bmatrix} -(d+\sigma+\beta I) & -(\beta S-\nu) & \nu_1 & 0 & 0 \\ \beta I & 0 & k_1 I & \beta_1 I & -k_1 I \\ 0 & k_1(H_a+H_b-H) & -(d+\theta\alpha+\nu_1+k_1 I) & 0 & k_1 I \\ \sigma & -\beta_1 V & 0 & -(d+\beta_1 I) & 0 \\ 0 & \phi & 0 & 0 & -\phi_0 \end{bmatrix}.$$

The characteristic polynomial of matrix J^* is obtained as

$$\Phi^5 + C_1\Phi^4 + C_2\Phi^3 + C_3\Phi^2 + C_4\Phi + C_5 = 0, \tag{4}$$

where

$$\begin{aligned}
C_1 &= 3d+\theta\alpha+\nu_1+\sigma+\phi_0+k_1I+\beta I+\beta_1 I,\\
C_2 &= -k_1^2I(H_a+H_b-H)+k_1\phi I+(d+\sigma+\beta I)(d+\beta_1 I)+\beta_1^2VI\\
&\quad+(d+\theta\alpha+\nu_1+\phi_0+k_1I)(2d+\sigma+\beta I+\beta_1 I)\\
&\quad+\phi_0(d+\theta\alpha+\nu_1+k_1I)+\beta I(\beta S-\nu),\\
C_3 &= -k_1^2I(H_a+H_b-H)(2d+\sigma+\phi_0+\beta I+\beta_1 I)\\
&\quad-\nu_1k_1\beta I(H_a+H_b-H)+k_1\phi I(3d+\theta\alpha+\nu_1+\sigma+\beta I+\beta_1 I)\\
&\quad+\beta_1^2VI(d+\sigma+\beta I)+(d+\theta\alpha+\nu_1+\phi_0+k_1I)\left[(d+\sigma+\beta I)(d\right.\\
&\quad\left.+\beta_1 I)+\beta_1^2VI\right]+\phi_0(d+\theta\alpha+\nu_1+k_1I)(2d+\sigma+\beta I+\beta_1 I)\\
&\quad+(\beta S-\nu)\left[\beta I(2d+\theta\alpha+\nu_1+\phi_0+k_1I+\beta_1 I)+\sigma\beta_1 I\right],\\
C_4 &= k_1\phi I\left[(d+\theta\alpha+\nu_1)(2d+\sigma+\beta I+\beta_1 I)+(d+\beta_1 I)(d+\sigma+\beta I)\right]\\
&\quad-\phi\nu_1\beta k_1I^2\\
&\quad-k_1^2I(H_a+H_b-H)\left[(\phi_0+d+\sigma+\beta I)(d+\beta_1 I)+\phi_0(d+\sigma+\beta I)\right]\\
&\quad-\nu_1k_1(H_a+H_b-H)\left[\beta I\phi_0+\beta I(d+\beta_1 I)\right]\\
&\quad+\beta_1^2VI(d+\sigma+\beta I)(d+\theta\alpha+\nu_1+\phi_0+k_1I)\\
&\quad+\phi_0(d+\theta\alpha+\nu_1+k_1I)\left[(d+\sigma+\beta I)(d+\beta_1 I)+\beta_1^2VI\right]\\
&\quad+(\beta S-\nu)(d+\theta\alpha+\nu_1+\phi_0+k_1I)\left[\beta I(d+\beta_1 I)+\sigma\beta_1 I\right]\\
&\quad+\phi_0\beta I(\beta S-\nu)(d+\theta\alpha+\nu_1+k_1I),\\
C_5 &= k_1\phi I(d+\theta\alpha+\nu_1)(d+\beta_1 I)(d+\sigma+\beta I)\\
&\quad-\phi\nu_1k_1I\left[\beta I(d+\beta_1 I)+\beta_1\sigma I\right]\\
&\quad-\phi_0k_1^2I(H_a+H_b-H)(d+\sigma+\beta I)(d+\beta_1 I)\\
&\quad-\phi_0\nu_1k_1(H_a+H_b-H)\left[\beta I(d+\beta_1 I)+\beta_1\sigma I\right]\\
&\quad+\beta_1^2\phi_0VI(d+\theta\alpha+\nu_1+k_1I)(d+\sigma+\beta I)\\
&\quad+\phi_0(\beta S-\nu)(d+\theta\alpha+\nu_1+k_1I)\left[\beta I(d+\beta_1 I)+\sigma\beta_1 I\right].
\end{aligned}$$

From the above expressions, it is clear that $C_1 > 0$. Thus, using Routh–Hurwitz criterion, we establish the following theorem.

Theorem 3. *The equilibrium E (E_1^* or E_2^*) is locally asymptotically stable if and only if all the principle minors of Routh–Hurwitz matrix of Eq. (4) (evaluated at E_1^* or E_2^*) are positive.*

4. Bifurcation analysis

4.1. Transcritical bifurcation

To determine possibility of the occurrence of transcritical bifurcation at $R_0 = 1$, we take the advantage of center manifold theory [28]. We consider $S = y_1$, $I = y_2$, $H = y_3$, $V = y_4$ and $H_b = y_5$; thus, the model system (2) can be written as

$$\begin{cases}
\frac{dy_1}{dt} = A-\beta y_1y_2-dy_1-\sigma y_1+\nu y_2+\nu_1y_3 := f_1,\\
\frac{dy_2}{dt} = \beta y_1y_2+\beta_1y_2y_4-(\nu+\alpha+d)y_2-k_1(H_a+y_5-y_3)y_2 := f_2,\\
\frac{dy_3}{dt} = k_1(H_a+y_5-y_3)y_2-(d+\theta\alpha+\nu_1)y_3 := f_3,\\
\frac{dy_4}{dt} = \sigma y_1-dy_4-\beta_1y_2y_4 := f_4,\\
\frac{dy_5}{dt} = \phi y_2-\phi_0y_5 := f_5.
\end{cases} \tag{5}$$

Here, we choose β as bifurcation parameter. Thus, the Jacobian matrix for model system (5) around E_0 at $\beta = \beta^*$ (or equivalently at $R_0 = 1$) can be expressed as

$$J_0 = \begin{bmatrix} -(d+\sigma) & -\beta^*\left(\frac{A}{d+\sigma}\right)+\nu & \nu_1 & 0 & 0 \\ 0 & 0 & 0 & 0 & 0 \\ 0 & k_1H_a & -(d+\theta\alpha+\nu_1) & 0 & 0 \\ \sigma & -\frac{\beta_1\sigma A}{d(d+\sigma)} & 0 & -d & 0 \\ 0 & \phi & 0 & 0 & -\phi_0 \end{bmatrix}.$$

The above matrix J_0 has a 0 eigenvalue and other four eigenvalues $-(d+\sigma)$, $-(d+\theta\alpha+\nu_1)$, $-d$, and $-\phi_0$ are negative.

Further, the right and left eigenvectors (respectively, $\tilde{V}$ and $\tilde{W}$) of matrix J_0 associated with eigenvalue 0 are obtained as

$$\tilde{V} = \begin{bmatrix} \tilde{v}_1 \\ \tilde{v}_2 \\ \tilde{v}_3 \\ \tilde{v}_4 \\ \tilde{v}_5 \end{bmatrix} = \begin{bmatrix} d\left[-\left(\frac{\beta^*A}{(d+\sigma)}-\nu\right)(d+\theta\alpha+\nu_1)+\nu_1k_1H_a\right] \\ d(d+\sigma)(d+\theta\alpha+\nu_1) \\ dk_1H_a(d+\sigma) \\ \sigma\left(-\left(\frac{\beta^*A}{(d+\sigma)}-\nu\right)(d+\theta\alpha+\nu_1)+\nu_1k_1H_a\right)-\frac{\beta_1\sigma A}{d}(d+\theta\alpha+\nu_1) \\ \frac{\phi}{\phi_0}d(d+\sigma)(d+\theta\alpha+\nu_1) \end{bmatrix},$$

$$\tilde{W} = \begin{bmatrix} \tilde{w}_1 \\ \tilde{w}_2 \\ \tilde{w}_3 \\ \tilde{w}_4 \\ \tilde{w}_5 \end{bmatrix}^T = \begin{bmatrix} 0 \\ 1 \\ 0 \\ 0 \\ 0 \end{bmatrix}^T.$$

Now, we compute the quantities a and b, mentioned in Theorem 4.1 of [28] for model system (2), that are obtained as follows

$$a = \sum_{i,j,k=1}^{5} \tilde{w}_k \tilde{v}_i \tilde{v}_j \frac{\partial^2 f_k}{\partial y_i \partial y_j}, \quad \text{and} \quad b = \sum_{i,k=1}^{5} \tilde{w}_k \tilde{v}_i \frac{\partial^2 f_k}{\partial y_i \partial \beta}.$$

Thus, we have

$$a = 2d(d+\sigma)(d+\theta\alpha+\nu_1)\left\{(\beta^* d + \beta_1\sigma)\left[-\left(\frac{\beta^* A}{(d+\sigma)} - \nu\right)(d+\theta\alpha+\nu_1) + \nu_1 k_1 H_a\right] - \frac{\beta_1^2\sigma A}{d}(d+\theta\alpha+\nu_1) + k_1^2 d H_a(d+\sigma) - \frac{\phi}{\phi_0}k_1 d(d+\sigma)(d+\theta\alpha+\nu_1)\right\},$$

and $b = A(d+\theta\alpha+\nu_1) > 0$. Now, if we put $a = 0$, we get

$$k_1^* = \frac{-\tilde{L}_1 + \sqrt{\tilde{L}_1^2 + 4dH_a(d+\sigma)\tilde{L}_2}}{2dH_a(d+\sigma)},$$

where $\tilde{L}_1 = \nu_1 H_a(\beta^* d + \beta_1\sigma) - \frac{\phi}{\phi_0}k_1(d+\sigma)(d+\theta\alpha+\nu_1)$, and $\tilde{L}_2 = (d+\theta\alpha+\nu_1)\left[(\beta^* d+\beta_1\sigma)\left(\frac{\beta^* A}{(d+\sigma)} - \nu\right) + \frac{\beta_1^2\sigma A}{d}\right]$. Thus, we establish the following theorem.

Theorem 4. *For $R_0 = 1$, the system (2) exhibits backward transcritical bifurcation if $k_1 > k_1^*$ and forward transcritical bifurcation if $k_1 < k_1^*$.*

4.2. Saddle–node bifurcation

Our aim here is to demonstrate the existence of saddle–node bifurcation for model system (2), for which we use Sotomayor's theorem [29]. Since R_0 is a function of β, we take β as a bifurcation parameter. From the above analysis, it is evident that model system (2) has a unique equilibrium E_3^* at $R_0 = R_0^*$ (or equitably $\beta = \beta_l$). Therefore, Jacobian matrix J_3^* (Jacobian matrix for model system (2) computed at E_3^*) has a eigenvalue 0, if $C_5(\beta_l) = 0$. Let $U_1 = (u_{11}, u_{21}, u_{31}, u_{41}, u_{51})^T$ and $U_2 = (u_{12}, u_{22}, u_{32}, u_{42}, u_{52})$, sequentially represent the left and right eigenvectors of matrix J_3^* associated with eigenvalue 0, where

$$\begin{aligned}
u_{11} &= (d+\beta_1 I_3^*)\left[-(\beta_l S_3^* - \nu)(d+\theta\alpha+\nu_1+k_1 I_3^*) + \nu_1 k_1\left(H_a + H_{b3}^* - H_3^* + \frac{\phi}{\phi_0} I_3^*\right)\right],\\
u_{21} &= (d+\beta_1 I_3^*)(d+\sigma+\beta_l I_3^*)(d+\theta\alpha+\nu_1+k_1 I_3^*),\\
u_{31} &= k_1(d+\beta_1 I_3^*)(d+\sigma+\beta_l I_3^*)\left(H_a + H_{b3}^* - H_3^* + \frac{\phi}{\phi_0} I_3^*\right),\\
u_{41} &= \sigma\left[-(\beta_l S_3^* - \nu)(d+\theta\alpha+\nu_1+k_1 I_3^*) + \nu_1 k_1\left(H_a + H_{b3}^* - H_3^* + \frac{\phi}{\phi_0} I_3^*\right)\right] - \beta_1 V_3^*(d+\sigma+\beta_l I_3^*)(d+\theta\alpha+\nu_1+k_1 I_3^*)\\
u_{51} &= \frac{\phi}{\phi_0}(d+\beta_1 I_3^*)(d+\sigma+\beta_l I_3^*)(d+\theta\alpha+\nu_1+k_1 I_3^*),\\
u_{12} &= \phi_0(d+\theta\alpha+\nu_1+k_1 I_3^*)\left[\beta_l I_3^*(d+\beta_1 I_3^*) + \sigma\beta_1 I_3^*\right],\\
u_{22} &= \phi_0(d+\beta_1 I_3^*)(d+\sigma+\beta_l I_3^*)(d+\theta\alpha+\nu_1+k_1 I_3^*),\\
u_{32} &= \phi_0\left[\nu_1\left(\beta_l I_3^*(d+\beta_1 I_3^*) + \sigma\beta_1 I_3^*\right) + k_1 I_3^*(d+\beta_1 I_3^*)(d+\sigma+\beta_l I_3^*)\right],\\
u_{42} &= \beta_1\phi_0 I_3^*(d+\sigma+\beta_l I_3^*)(d+\theta\alpha+\nu_1+k_1 I_3^*),\\
u_{52} &= -k_1 I_3^*(d+\beta_1 I_3^*)(d+\sigma+\beta_l I_3^*)(d+\theta\alpha+\nu_1+k_1 I_3^*) + k_1 I_3^*\left[\nu_1\left(\beta_l I_3^*(d+\beta_1 I_3^*) + \sigma\beta_1 I_3^*\right) + k_1 I_3^*(d+\beta_1 I_3^*)(d+\sigma+\beta_l I_3^*)\right].
\end{aligned}$$

Let $\hat{\mathfrak{G}} = \left(\hat{\mathfrak{G}}_1, \hat{\mathfrak{G}}_2, \hat{\mathfrak{G}}_3, \hat{\mathfrak{G}}_4, \hat{\mathfrak{G}}_5\right)$, where $\hat{\mathfrak{G}}_1$, $\hat{\mathfrak{G}}_2$, $\hat{\mathfrak{G}}_3$, $\hat{\mathfrak{G}}_4$ and $\hat{\mathfrak{G}}_5$ are right hand sides of $\frac{dS}{dt}$, $\frac{dI}{dt}$, $\frac{dH}{dt}$, $\frac{dV}{dt}$, and $\frac{dH_b}{dt}$, respectively in model system (2). Then

$$\mathscr{B}_1 = U_2.\frac{d\hat{\mathfrak{G}}}{d\beta}\Big|_{(E_3^*,\beta_l)} = \phi_0 d S_3^* I_3^*(d+\sigma+\beta_1 I_3^*)(d+\theta\alpha+\nu_1+k_1 I_3^*) > 0,$$

and

$$\begin{aligned}
\mathscr{B}_2 &= U_2.\left[D^2_{(S,I,H,V,H_b)}\hat{\mathfrak{G}}(U_1,U_1)\right]\Big|_{(E_3^*,\beta_l)}\\
&= 2u_{21}[\beta_l u_{11}(u_{32}-u_{12}) + \beta_1 u_{41}(u_{32}-u_{42})].
\end{aligned}$$

Therefore, if $\mathscr{B}_2 \neq 0$, then the conditions of Sotomayor's theorem are met for the existence of saddle–node bifurcation. Thus, we state the following theorem.

Theorem 5. *For $R_0 = R_0^*$, the model system (2) undergoes a saddle–node bifurcation at equilibrium E_3^*, provided $\mathscr{B}_2 \neq 0$.*

4.3. Existence of Hopf bifurcation

To show that model system (2) experiences Hopf bifurcation at equilibrium E_1^*, we choose β as a bifurcation parameter. Since all the coefficients of characteristic Eq. (4) can be expressed as a function of β; therefore, we have

$$\Phi^5 + C_1(\beta)\Phi^4 + C_2(\beta)\Phi^3 + C_3(\beta)\Phi^2 + C_4(\beta)\Phi + C_5(\beta) = 0. \tag{6}$$

The Eq. (6) has a pair of purely imaginary solutions $\Phi_{1,2} = \pm i\sqrt{\xi_0}$, $\xi_0 > 0$ if and only if it can be written as

$$\mathcal{Q}(\Phi) = (\Phi^2 + \xi_0)\mathcal{G}(\Phi), \text{ where } \mathcal{G}(\Phi) = \Phi^3 + \mathcal{L}_1\Phi^2 + \mathcal{L}_2\Phi + \mathcal{L}_3.$$

Thus, we have

$$\mathcal{Q}(\Phi) = \Phi^5 + \mathcal{L}_1\Phi^4 + (\mathcal{L}_2+\xi_0)\Phi^3 + (\mathcal{L}_3 + \mathcal{L}_1\xi_0)\Phi^2 + \mathcal{L}_2\xi_0\Phi + \mathcal{L}_3\xi_0. \tag{7}$$

Equating the coefficients of Eqs. (6) and (7), we have

$$C_1 = \mathcal{L}_1,\ C_2 = \mathcal{L}_2 + \xi_0,\ C_3 = \mathcal{L}_3 + \mathcal{L}_1\xi_0,\ C_4 = \mathcal{L}_2\xi_0, \text{ and } C_5 = \mathcal{L}_3\xi_0.$$

For the consistence of above relations, we have

$$\xi_0^2 - C_2\xi_0 + C_4 = 0,\ C_1\xi_0^2 - C_3\xi_0 + C_5 = 0.$$

The elimination of ξ_0^2 gives

$$(C_3 - C_1C_2)\xi_0 = C_5 - C_1C_4. \tag{8}$$

Thus, Eq. (6) can be written as

$$\mathcal{Q}(\Phi) = \Phi^5 + C_1\Phi^4 + C_2\Phi^3 + C_3\Phi^2 + \xi_0(C_2-\xi_0)\Phi + \xi_0(C_3 - C_1\xi_0). \tag{9}$$

If $(C_3 - C_1C_2)(C_5 - C_1C_4) > 0$, then from Eq. (8), we have

$$\xi_0 = \xi_0^* = \frac{C_5 - C_1C_4}{C_3 - C_1C_2} > 0.$$

Substituting $\xi_0 = \xi_0^*$ in Eq. (9), we find that Eqs. (6) and (9) are identical if and only if

$$\varphi = (C_3 - C_1C_2)(C_5C_2 - C_3C_4) - (C_5 - C_1C_4)^2 = 0.$$

Thus, the necessary and sufficient conditions under which the polynomial $\mathcal{G}(\Phi) = \Phi^3 + C_1\Phi^2 + (C_2-\xi_0)\Phi + C_3 - C_1\xi_0$ does not have zero solution is

$$C_3 - C_1\xi_0 \neq 0.$$

The polynomial $\mathcal{G}(\phi)$ has all solutions with negative real parts if and only if all leading principal minors of the matrix

$$\begin{bmatrix} \mathcal{L}_1 & \mathcal{L}_3 & 0 \\ 1 & \mathcal{L}_2 & 0 \\ 0 & \mathcal{L}_1 & \mathcal{L}_3 \end{bmatrix} = \begin{bmatrix} C_1 & C_3 - C_1\xi_0 & 0 \\ 1 & C_2 - \xi_0 & 0 \\ 0 & C_1 & C_3 - C_1\xi_0 \end{bmatrix}$$

are positive (i.e., the conditions of Routh–Hurwitz criterion are satisfied). The positivity of the determinants leads to the conditions

$$C_1 > 0,\ C_1C_2 - C_3 > 0,\ C_3 - C_1\xi_0 > 0.$$

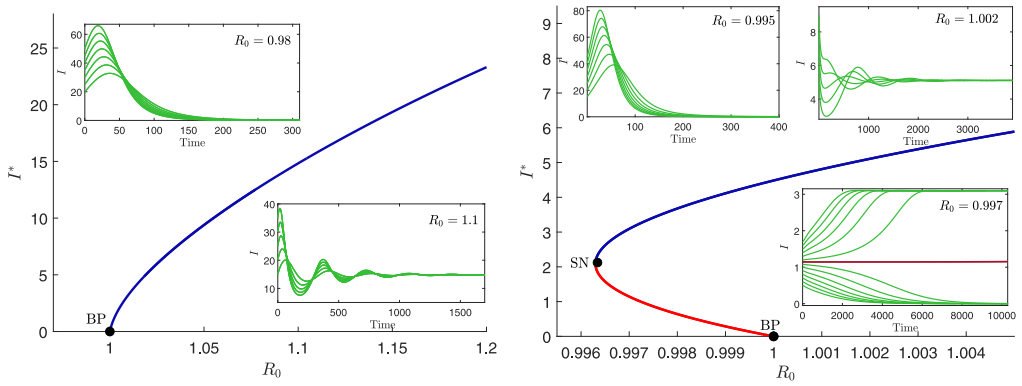

Fig. 3. Bifurcation plots in $R_0 - I^*$ plane for (a) $k_1 = 0.00085$ (b) $k_1 = 0.001$.

To complete the discussion, it remains to verify the transversality condition. The function $\varphi(\beta)$ can be expressed in the form of Orlando's formula as

$$\varphi(\beta) = (\Phi_1+\Phi_2)(\Phi_1+\Phi_3)(\Phi_1+\Phi_4)(\Phi_1+\Phi_5)(\Phi_2+\Phi_3)$$
$$(\Phi_2+\Phi_4)(\Phi_2+\Phi_5)(\Phi_3+\Phi_4)(\Phi_3+\Phi_5)(\Phi_4+\Phi_5).$$

As $\varphi(\beta_l)$ is a continuous function of all its solutions, there exists an open interval $X_{\beta_l} = (\beta_l - \delta, \beta_l + \delta)$, where Φ_1 and Φ_2 are complex conjugates for all $\beta \in X_{\beta_l}$. Let there general form in this neighborhood be $\Phi_1(\beta) = \xi_1(\beta) + i\xi_2(\beta)$, $\Phi_2(\beta) = \xi_1(\beta) - i\xi_2(\beta)$ with $\xi_1(\beta_l) = 0$, and $\xi_2(\beta_l) = \sqrt{\xi_0} > 0$, while $Re\{\Phi_{3,4,5}(\beta_l)\} \neq 0$. Then, we have

$$\varphi(\beta) = 2\xi_1\left\{(\Phi_3+\xi_1)^2+\xi_2^2\right\}\left\{(\Phi_4+\xi_1)^2+\xi_2^2\right\}\left\{(\Phi_5+\xi_1)^2+\xi_2^2\right\}$$
$$(\Phi_3+\Phi_4)(\Phi_3+\Phi_4)(\Phi_4+\Phi_5), \quad \varphi(\beta_l) = 0.$$

Differentiating with respect to β and putting $\beta = \beta_l$, we obtain

$$\left[\frac{d\varphi(\beta)}{d\beta}\right]_{\beta=\beta_l} = \left[2(\xi_2^2+\Phi_3^2)(\xi_2^2+\Phi_4^2)(\xi_2^2+\Phi_5^2)(\Phi_3+\Phi_4)\right.$$
$$\left.(\Phi_3+\Phi_5)(\Phi_4+\Phi_5)\frac{d\xi_1(\beta)}{d\beta}\right]_{\beta=\beta_l}.$$

Since the solutions $\Phi_{3,4,5}$ have negative real parts at $\beta = \beta_l$, therefore

$$\left[\frac{d\xi_1(\beta)}{d\beta}\right]_{\beta=\beta_l} \neq 0 \Longleftrightarrow \left[\frac{d\varphi(\beta)}{d\beta}\right]_{\beta=\beta_l} \neq 0.$$

Thus, the transversality condition holds and we establish the following theorem.

Theorem 6. *When the disease transmission rate β exceeds the critical value β_l, the proposed system (2) enters into Hopf bifurcation around the endemic equilibrium E_1^* if the following necessary and sufficient conditions are satisfied.*

$$\begin{cases} (a)\ \ \varphi(\beta_l) = \left[C_3(\beta_l) - C_1(\beta_l)C_2(\beta_l)\right]\left[C_5(\beta_l)C_2(\beta_l) - C_3(\beta_l)C_4(\beta_l)\right] \\ \qquad - \left[C_5(\beta_l) - C_1(\beta_l)C_4(\beta_l)\right] = 0, \\ (b)\ \ C_1(\beta_l) > 0,\ C_1(\beta_l)C_2(\beta_l) - C_3(\beta_l) > 0,\ C_3(\beta_l) - C_1(\beta_l)\xi_0^* > 0, \\ \qquad \xi_0^* = \dfrac{C_5(\beta_l) - C_1(\beta_l)C_4(\beta_l)}{C_3(\beta_l) - C_1(\beta_l)C_2(\beta_l)} > 0, \\ (c)\ \ \left[\dfrac{d\varphi(\beta)}{d\beta}\right]_{\beta=\beta_l} \neq 0. \end{cases}$$

4.4. Bogdanov–Takens bifurcation

From Theorem 2, it is clear that endemic equilibria $E_1^*(S_1^*, I_1^*, H_1^*, V_1^*, H_{b1}^*)$ and $E_2^*(S_2^*, I_2^*, H_2^*, V_2^*, H_{b2}^*)$ collide and unite into equilibrium $E_3^*(S_3^*, I_3^*, H_3^*, V_3^*, H_{b3}^*)$ at $R_0 = R_0^*$. Thus, there is a possibility for the existence of Bogdanov–Takens (BT) bifurcation of co-dimension 2 at equilibrium E_3^*. Therefore, to determine the conditions under which proposed system experiences BT bifurcation of co-dimension 2, we use the transformation $\hat{S} = S - S_3^*$, $\hat{I} = I - I_3^*$, $\hat{H} = H - H_3^*$, $\hat{V} = V - V_3^*$ and $\hat{H}_b = H_b - H_{b3}^*$. Thus, we get

$$\begin{bmatrix} \hat{S} \\ \hat{I} \\ \hat{H} \\ \hat{V} \\ \hat{H}_b \end{bmatrix}' = J_3^* \begin{bmatrix} \hat{S} \\ \hat{I} \\ \hat{H} \\ \hat{V} \\ \hat{H}_b \end{bmatrix} + \begin{bmatrix} -\beta\hat{S}\hat{I} \\ \beta\hat{S}\hat{I} + \beta_1\hat{V}\hat{I} - k_1\left(\tilde{H}_b - \hat{H}\right)\hat{I} \\ k_1\left(\tilde{H}_b - \hat{H}\right)\hat{I} \\ -\beta_1\hat{V}\hat{I} \\ 0 \end{bmatrix}. \tag{10}$$

If $C_4(E_3^*) = C_5(E_3^*) = 0$, then the matrix J_3^* (Jacobian matrix for model system (2) evaluated at E_3^*) has zero eigenvalue with algebraic multiplicity 2. For this analysis, we use $a_1 = d + \theta\alpha + \nu_1 + k_1 I_3^*$ and $a_2 = d + \beta_1 I_3^*$. Now, the generalized eigenvectors associated with eigenvalues $\Phi_{1,2} = 0$ are $\hat{V}_1 = \left[\hat{v}_{11}, \hat{v}_{21}, \hat{v}_{31}, \hat{v}_{41}, \hat{v}_{51}\right]^T$ and $\hat{V}_2 = \left[\hat{v}_{12}, \hat{v}_{22}, \hat{v}_{32}, \hat{v}_{42}, 0\right]^T$, where

$$\hat{v}_{11} = a_2\left[-a_1(\beta S_3^* - \nu) + \nu_1\left(k_1(H_a + H_{b3}^* - H_3^*) + k_1\frac{\phi}{\phi_0}I_3^*\right)\right],$$

$$\hat{v}_{21} = a_1a_2(d+\sigma+\beta I_3^*),\ \ \hat{v}_{31} = a_2(d+\sigma+\beta I_3^*)\left[k_1(H_a + H_{b3}^* - H_3^*) + k_1\frac{\phi}{\phi_0}I_3^*\right],$$

$$\hat{v}_{41} = -\beta a_1 V_3^*(d+\sigma+\beta I_3^*) + \sigma\left[-a_1(\beta S_3^* - \nu)\right.$$
$$\left. + \nu_1\left(k_1(H_a + H_{b3}^* - H_3^*) + k_1\frac{\phi}{\phi_0}I_3^*\right)\right],\ \ \hat{v}_{51} = a_1a_2\frac{\phi}{\phi_0}(d+\sigma+\beta I_3^*),$$

$$\hat{v}_{12} = a_2\left[-a_1(\beta S_3^* - \nu)\hat{v}_{51} + \nu_1\left(k_1(H_a + H_{b3}^* - H_3^*)\hat{v}_{51} - \phi\hat{v}_{31}\right) - \phi a_1\hat{v}_{11}\right],$$

$$\hat{v}_{22} = a_1a_2(d+\sigma+\beta I_3^*)\hat{v}_{51},$$

$$\hat{v}_{32} = a_2(d+\sigma+\beta I_3^*)\left[k_1(H_a + H_{b3}^* - H_3^*)\hat{v}_{51} - \phi\hat{v}_{31}\right],$$

$$\hat{v}_{42} = \sigma\left[-a_1(\beta S_3^* - \nu)\hat{v}_{51} + \nu_1\left(k_1(H_a + H_{b3}^* - H_3^*)\hat{v}_{51} - \phi\hat{v}_{31}\right) - \phi a_1\hat{v}_{11}\right]$$
$$- \beta_1 V_3^* a_1(d+\sigma+\beta I_3^*)\hat{v}_{51}.$$

Now, the eigenvectors corresponding to the eigenvalues Φ_3, Φ_4 and Φ_5 are $\hat{V}_3 = \left[\hat{v}_{13}, \hat{v}_{23}, \hat{v}_{33}, \hat{v}_{43}, \hat{v}_{53}\right]^T$, $\hat{V}_4 = \left[\hat{v}_{14}, \hat{v}_{24}, \hat{v}_{34}, \hat{v}_{44}, \hat{v}_{54}\right]^T$, and $\hat{V}_5 = \left[\hat{v}_{15}, \hat{v}_{25}, \hat{v}_{35}, \hat{v}_{45}, \hat{v}_{55}\right]^T$, where

$$\hat{v}_{13} = (a_2+\Phi_3)\left[-(a_1+\Phi_3)(\phi_0+\Phi_3)(\beta S_3^* - \nu)\right.$$
$$\left. + \nu_1\left(k_1(H_a + H_{b3}^* - H_3^*)(\phi_0+\Phi_3) + k_1\phi I_3^*\right)\right],$$

$$\hat{v}_{23} = (a_1+\Phi_3)(a_2+\Phi_3)(\phi_0+\Phi_3)(d+\sigma+\Phi_3+\beta I_3^*),$$

$$\hat{v}_{33} = (a_2+\Phi_3)(d+\sigma+\Phi_3+\beta I_3^*)\left[k_1(H_a + H_{b3}^* - H_3^*)(\phi_0+\Phi_3) + k_1\phi I_3^*\right],$$

$$\hat{v}_{43} = -\beta V_3^*(a_1+\Phi_3)(\phi_0+\Phi_3)(d+\sigma+\Phi_3+\beta I_3^*)$$
$$+ \sigma\left[-(a_1+\Phi_3)(\phi_0+\Phi_3)(\beta S_3^* - \nu) + \nu_1\left(k_1(H_a + H_{b3}^* - H_3^*)(\phi_0+\Phi_3) + k_1\phi I_3^*\right)\right],$$

$$\hat{v}_{53} = \phi(a_1+\Phi_3)(a_2+\Phi_3)(d+\sigma+\Phi_3+\beta I_3^*),$$

$$\hat{v}_{14} = (a_2+\Phi_4)\left[-(a_1+\Phi_4)(\phi_0+\Phi_4)(\beta S_3^*-\nu) + \nu_1\left(k_1(H_a+H_{b3}^*-H_3^*)(\phi_0+\Phi_4)+k_1\phi I_3^*\right)\right],$$
$$\hat{v}_{24} = (a_1+\Phi_4)(a_2+\Phi_4)(\phi_0+\Phi_4)(d+\sigma+\Phi_4+\beta I_3^*),$$
$$\hat{v}_{34} = (a_2+\Phi_4)(d+\sigma+\Phi_4+\beta I_3^*)\left[k_1(H_a+H_{b3}^*-H_3^*)(\phi_0+\Phi_4)+k_1\phi I_3^*\right],$$
$$\hat{v}_{44} = -\beta V_3^*(a_1+\Phi_4)(\phi_0+\Phi_4)(d+\sigma+\Phi_4+\beta I_3^*) + \sigma\left[-(a_1+\Phi_4)(\phi_0+\Phi_4)(\beta S_3^*-\nu)+\nu_1\left(k_1(H_a+H_{b3}^*-H_3^*)(\phi_0+\Phi_4)+k_1\phi I_3^*\right)\right],$$

$$\hat{v}_{54} = \phi(a_1+\Phi_4)(a_2+\Phi_4)(d+\sigma+\Phi_4+\beta I_3^*),$$
$$\hat{v}_{15} = (a_2+\phi_5)\left[-(a_1+\Phi_5)(\phi_0+\Phi_5)(\beta S_3^*-\nu) + \nu_1\left(k_1(H_a+H_{b3}^*-H_3^*)(\phi_0+\Phi_5)+k_1\phi I_3^*\right)\right],$$
$$\hat{v}_{25} = (a_1+\phi_5)(a_2+\Phi_5)(\phi_0+\Phi_5)(d+\sigma+\Phi_5+\beta I_3^*),$$
$$\hat{v}_{35} = (a_2+\Phi_5)(d+\sigma+\Phi_5+\beta I_3^*)\left[k_1(H_a+H_{b3}^*-H_3^*)(\phi_0+\Phi_5)+k_1\phi I_3^*\right],$$
$$\hat{v}_{45} = -\beta V_3^*(a_1+\Phi_5)(\phi_0+\Phi_5)(d+\sigma+\Phi_5+\beta I_3^*) + \sigma\left[-(a_1+\Phi_5)(\phi_0+\Phi_5)(\beta S_3^*-\nu)+\nu_1\left(k_1(H_a+H_{b3}^*-H_3^*)(\phi_0+\Phi_5)+k_1\phi I_3^*\right)\right],$$
$$\hat{v}_{55} = \phi(a_1+\Phi_5)(a_2+\Phi_5)(d+\sigma+\Phi_5+\beta I_3^*).$$

Now, we consider $\hat{M} = \left[\hat{\mathrm{V}}_1, \hat{\mathrm{V}}_2, \hat{\mathrm{V}}_3, \hat{\mathrm{V}}_4, \hat{\mathrm{V}}_5\right]$ and use the following non-singular transformation to reduce the system (10)

$$\begin{bmatrix} \hat{S} \\ \hat{I} \\ \hat{H} \\ \hat{V} \\ \hat{H}_b \end{bmatrix} = \hat{M} \begin{bmatrix} \hat{Y}_1 \\ \hat{Y}_2 \\ \hat{Y}_3 \\ \hat{Y}_4 \\ \hat{Y}_5 \end{bmatrix}.$$

Let the inverse of matrix $\hat{M}$ is given by $\hat{M}^{-1} = \begin{bmatrix} \hat{m}_{11} & \hat{m}_{12} & \hat{m}_{13} & \hat{m}_{14} & \hat{m}_{15} \\ \hat{m}_{21} & \hat{m}_{22} & \hat{m}_{23} & \hat{m}_{24} & \hat{m}_{25} \\ \hat{m}_{31} & \hat{m}_{32} & \hat{m}_{33} & \hat{m}_{34} & \hat{m}_{35} \\ \hat{m}_{41} & \hat{m}_{42} & \hat{m}_{43} & \hat{m}_{44} & \hat{m}_{45} \\ \hat{m}_{51} & \hat{m}_{52} & \hat{m}_{53} & \hat{m}_{54} & \hat{m}_{55} \end{bmatrix}$. Then, the system (10) becomes

$$\begin{cases} \hat{Y}_1' = \hat{Y}_2 + \hat{P}_{20}\hat{Y}_1^2 + \hat{P}_{11}\hat{Y}_1\hat{Y}_2 + \hat{P}_{02}\hat{Y}_2^2 + \mathcal{O}\left(\left|\hat{Y}_1,\hat{Y}_2,\hat{Y}_3,\hat{Y}_4,\hat{Y}_5\right|^2\right), \\ \hat{Y}_2' = \hat{Q}_{20}\hat{Y}_1^2 + \hat{Q}_{11}\hat{Y}_1\hat{Y}_2 + \hat{Q}_{02}\hat{Y}_2^2 + \mathcal{O}\left(\left|\hat{Y}_1,\hat{Y}_2,\hat{Y}_3,\hat{Y}_4,\hat{Y}_5\right|^2\right), \\ \hat{Y}_3' = \phi_3\hat{Y}_3 + \mathcal{O}\left(\left|\hat{Y}_1,\hat{Y}_2,\hat{Y}_3,\hat{Y}_4,\hat{Y}_5\right|^2\right), \\ \hat{Y}_4' = \phi_4\hat{Y}_4 + \mathcal{O}\left(\left|\hat{Y}_1,\hat{Y}_2,\hat{Y}_3,\hat{Y}_4,\hat{Y}_5\right|^2\right), \\ \hat{Y}_5' = \phi_5\hat{Y}_5 + \mathcal{O}\left(\left|\hat{Y}_1,\hat{Y}_2,\hat{Y}_3,\hat{Y}_4,\hat{Y}_5\right|^2\right), \end{cases} \tag{11}$$

where

$$\hat{P}_{20} = -\beta\hat{m}_{11}\hat{v}_{11}\hat{v}_{21} + k_1\hat{m}_{13}\hat{v}_{21}(\hat{v}_{51}-\hat{v}_{31}) - \beta_1\hat{m}_{14}\hat{v}_{41}\hat{v}_{21},$$
$$\hat{P}_{11} = -\beta\hat{m}_{11}(\hat{v}_{11}\hat{v}_{22}+\hat{v}_{12}\hat{v}_{21}) + \hat{m}_{12}\hat{v}_{21}(\beta\hat{v}_{12}+\beta_1\hat{v}_{42}+k_1\hat{v}_{32}) + \hat{m}_{13}\left[k_1\hat{v}_{22}(\hat{v}_{51}-\hat{v}_{31}) - k_1\hat{v}_{32}\hat{v}_{21}\right] - \beta_1\hat{m}_{14}(\hat{v}_{41}\hat{v}_{22}+\hat{v}_{41}\hat{v}_{21}),$$
$$\hat{P}_{02} = -\beta\hat{m}_{11}\hat{v}_{12}\hat{v}_{22} + \hat{m}_{12}\hat{v}_{22}(\beta\hat{v}_{12}+\beta_1\hat{v}_{42}+k_1\hat{v}_{32}) - k_1\hat{m}_{13}\hat{v}_{22}\hat{v}_{32} - \beta_1\hat{m}_{14}\hat{v}_{42}\hat{v}_{22},$$
$$\hat{Q}_{20} = -\beta\hat{m}_{21}\hat{v}_{11}\hat{v}_{21} + k_1\hat{m}_{23}\hat{v}_{21}(\hat{v}_{51}-\hat{v}_{31}) - \beta_1\hat{m}_{24}\hat{v}_{41}\hat{v}_{21},$$
$$\hat{Q}_{11} = -\beta\hat{m}_{21}(\hat{v}_{11}\hat{v}_{22}+\hat{v}_{12}\hat{v}_{21}) + \hat{m}_{22}\hat{v}_{21}(\beta\hat{v}_{12}+\beta_1\hat{v}_{42}+k_1\hat{v}_{32}) + \hat{m}_{23}\left[k_1\hat{v}_{22}(\hat{v}_{51}-\hat{v}_{31}) - k_1\hat{v}_{32}\hat{v}_{21}\right] - \beta_1\hat{m}_{24}(\hat{v}_{41}\hat{v}_{22}+\hat{v}_{41}\hat{v}_{21}),$$
$$\hat{Q}_{02} = -\beta\hat{m}_{21}\hat{v}_{12}\hat{v}_{22} + \hat{m}_{22}\hat{v}_{22}(\beta\hat{v}_{12}+\beta_1\hat{v}_{42}+k_1\hat{v}_{32}) - k_1\hat{m}_{23}\hat{v}_{22}\hat{v}_{21} - \beta_1\hat{m}_{24}\hat{v}_{42}\hat{v}_{22}.$$

The system (11) confined to the center manifold.

$$\begin{cases} \hat{Y}_1' = \hat{Y}_2 + \hat{P}_{20}\hat{Y}_1^2 + \hat{P}_{11}\hat{Y}_1\hat{Y}_2 + \hat{P}_{02}\hat{Y}_2^2 + \mathcal{O}\left(\left|\hat{Y}_1,\hat{Y}_2\right|^2\right), \\ \hat{Y}_2' = \hat{Q}_{20}\hat{Y}_1^2 + \hat{Q}_{11}\hat{Y}_1\hat{Y}_2 + \hat{Q}_{02}\hat{Y}_2^2 + \mathcal{O}\left(\left|\hat{Y}_1,\hat{Y}_2\right|^2\right). \end{cases} \tag{12}$$

Considering the near-identity transformation

$$\begin{cases} \hat{Y}_1 = \hat{\mathcal{W}} + \frac{1}{2}\left(\hat{P}_{11}+\hat{Q}_{02}\right)\hat{\mathcal{W}}^2 + \hat{P}_{02}\tilde{\mathcal{W}}\hat{\mathcal{V}} + \mathcal{O}\left(\left|\tilde{\mathcal{W}},\hat{\mathcal{V}}\right|^2\right), \\ \hat{Y}_2 = \hat{\mathcal{V}} - \tilde{P}_{20}\hat{\mathcal{W}}^2 + \hat{Q}_{02}\tilde{\mathcal{W}}\hat{\mathcal{V}} + \mathcal{O}\left(\left|\hat{\mathcal{W}},\hat{\mathcal{V}}\right|^2\right), \end{cases}$$

and re-write the system (12) in $\hat{Y}_1$ and $\hat{Y}_2$, we obtain

$$\begin{cases} \hat{Y}_1' = \hat{Y}_2, \\ \hat{Y}_2' = \hat{\mathscr{Q}}_{20}\hat{Y}_1^2 + \hat{\mathscr{Q}}_{11}\hat{Y}_1\hat{Y}_2 + \mathcal{O}\left(\left|\hat{Y}_1,\hat{Y}_2\right|^2\right). \end{cases}$$

Here, $\hat{\mathscr{Q}}_{20} = \hat{Q}_{20}$ and $\hat{\mathscr{Q}}_{11} = \hat{P}_{11} + 2\hat{P}_{20}$. Thus, we establish the following theorem.

Theorem 7. *The model system (2) exhibits BT bifurcation of co-dimension 2 around the equilibrium E_3^* provided $\hat{\mathscr{Q}}_{20} \neq 0$ and $\hat{\mathscr{Q}}_{11} \neq 0$.*

5. Numerical simulations

To conduct the numerical simulations for the model system (2), we take a set of parameter values, given in Table 3, for which $R_0 \approx 1.2967$ and the components of unique endemic equilibrium E_1^* are

$$S_1^* \approx 382, \quad I_1^* \approx 32, \quad H_1^* \approx 123, \quad V_1^* \approx 745, \quad \text{and} \quad H_{b1}^* \approx 72.$$

The eigenvalues of Jacobian matrix J^* are obtained as

$$-0.0092,\ -0.0095-0.033i, -0.0095+0.033i,\ -0.047-0.010i, \text{ and } -0.047+0.010i.$$

We note that one eigenvalue is negative and other four eigenvalues have negative real parts, which guarantees the local stability of unique endemic equilibrium E_1^*.

5.1. Bifurcation results

In this section, we provide the bifurcation diagrams in Figs. 3–10 to substantiate the analytically obtained bifurcation results. At point 'BP', transcritical bifurcation occurs, where disease-free equilibrium changes its stability to endemic equilibrium. Point 'SN' represents the occurrence of saddle–node bifurcation. This phenomenon of saddle–node bifurcation represents the collision and disappearance of two endemic equilibria. The Hopf bifurcation point is represented by 'H', where limit cycle (stable or unstable) originates from or ceases at the Hopf bifurcation point. Further, point 'LPC' represents limit cycle bifurcation, where two limit cycles (one stable and one unstable) collide and annihilate each other. The point 'BT' denotes the BT bifurcation of co-dimension 2. Around this point, three co-dimension 1 bifurcations occur: saddle–node, Hopf and homoclinic bifurcation. The homoclinic bifurcation is represented by 'Hom'. This is the point, where limit cycle (stable or unstable) collides with a saddle equilibrium and ceases to appear. The point 'GH', represents generalized Hopf bifurcation. This point separates the branches of supercritical and subcritical Hopf bifurcations in the parametric plane. For nearby parameter values, model system (2) demonstrates two limit cycles that come into collision and annihilate each other via saddle–node bifurcation.

(a) *Transcritical bifurcation:* We first study the effect of hospitalization rate coefficient k_1 on model system (2) with bifurcation parameter R_0 (obtained by varying β). For this, we have plotted the equilibrium curve in $R_0 - I^*$ plane for different values of k_1. For $k_1 = 0.00085$, equilibrium curve shows the transcritical bifurcation in forward direction at $R_0 = 1$, Fig. 3(a), which insinuates that disease-free equilibrium changes its stability at $R_0 = 1$.

Biologically, for $k_1 = 0.00085$, we can infer that if $R_0 < 1$ (which can be achieved either by increasing the number of hospital beds or by increasing the vaccination rate), the disease can be rooted out from the population. The increase in hospital beds reduces the waiting time of

Table 3
Parameters' description of proposed system (2) and their values used in numerical simulations.

Parameter	Description	Value
A	Immigration rate	20 person day^{-1}
d	Natural mortality rate	0.0105 day^{-1}
k_1	Hospitalization rate coefficient	0.001 day^{-1}
β	Transferral rate of individuals from susceptible to infected class	0.000392 person^{-1} day^{-1}
β_1	Transferral rate of individuals from vaccinated to infected class	0.00015 person^{-1} day^{-1}
ν_1	Hospital recovery rate	0.0025 day^{-1}
H_a	Number of hospital beds	100
α	Disease induced death rate	0.2 day^{-1}
σ	Vaccination rate	0.03 day^{-1}
ν	Self recovery rate	0.002 day^{-1}
θ	Disease induced mortality coefficient of hospitalized individuals	0.0001
ϕ	Rate of increasing new hospital beds	0.02 day^{-1}
ϕ_0	Rate at which new hospital beds reduces	0.009 day^{-1}

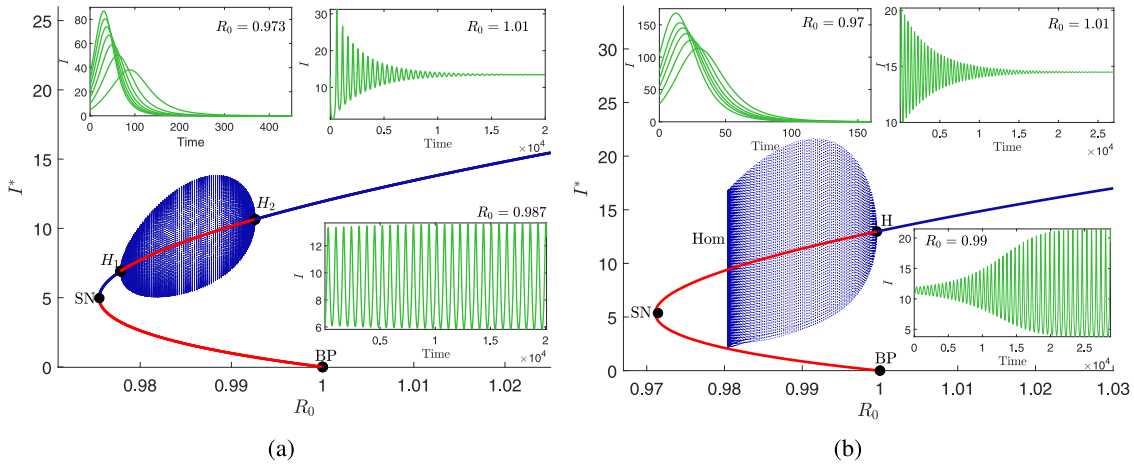

Fig. 4. Bifurcation plot in $R_0 - I^*$ plane for (a) $k_1 = 0.001215$ (b) $k_1 = 0.00125$.

infected individuals to get the treatment, also increase in vaccination rate drives more susceptible population to vaccinated class, which can reduce the transmission rate and hence the disease prevalence. Further, for $k_1 = 0.001$, the transcritical bifurcation changes its direction to backward, Fig. 3(b), which indicates that $R_0 < 1$ is not enough to eliminate the disease. Thus, to eradicate the disease from the population, more efforts are needed to push R_0 less than threshold $R_0^* = 0.9965$. Moreover, if $R_0 \in (0.9965, 1)$, the eradication or prevalence of the disease depends on the initial size of the infected population, which is shown through variation plot with respect to time 't' for $R_0 = 0.997 \in (0.9965, 1)$.

(b) *Supercritical Hopf bifurcation:* For $k_1 = 0.001215$, the model system (2) exhibits two Hopf-points H_1 ($R_0 \approx 0.9778$) and H_2 ($R_0 \approx 0.9926$). Between these two critical values of R_0, the model system (2) demonstrates a self-excited stable oscillatory solution, which means that there will be a periodic outbreak of epidemic whenever $R_0 \in (0.9778, 0.9926)$, Fig. 4(a). We observed that due to the presence of a stable limit cycle, the number of infected individuals oscillates in a range dependent on the amplitude of the stable limit cycle. Since the number of infected individuals fluctuates continuously, healthcare managers and policymakers will have difficulties in making strategies to diminish its prevalence. Further, for $k_1 = 0.00125$, the model system (2) again exhibits a stable limit cycle via supercritical Hopf bifurcation at $R_0 \approx 0.9996$, which ceases to appear through homoclinic bifurcation, Fig. 4(b).

(c) *Subcritical Hopf bifurcation and limit cycle bifurcation:* For $k_1 = 0.0016$, the proposed model system (2) enters into limit cycle oscillations via subcritical Hopf bifurcation, Fig. 5(a). From this figure, we observe that when $R_0 \in (0.9882, 0.9902)$, the unstable endemic equilibrium surrounds itself with a stable limit cycle. Further, this unstable endemic equilibrium turns into stable focus and covers itself with one unstable and one stable limit cycle when $R_0 \in (0.9902, 0.9938)$. These two limit cycles dissipate by colliding each other at $R_0 \approx 0.9938$. For $R_0 \in (0.9882, 0.9938)$, the solution trajectories either approach to stable focus or stable disease-free equilibrium or the periodic fluctuations arise, according to the initial values of infected population. Therefore, for $R_0 \in (0.9882, 0.9938)$, this complex behavior depicts that either the disease persists or dies out from the community depends on the initial size of infected population. To understand this complicated dynamics when $R_0 \in (0.9882, 0.9938)$, we sequentially plot phase portraits in $S - I - V$ space for $R_0 = 0.989$ and $R_0 = 0.991$ in Figs. 5(b) and 5(c). From Fig. 5(b), one can note that the solution trajectory (green curve) approaches to disease-free equilibrium and the solution trajectory (blue curve) spiral outward to the stable limit cycle (black curve) as $t \to \infty$. Moreover, for $R_0 = 0.991$, system (2) generates one stable limit cycle (black curve) and one unstable limit cycle (between red and blue curves), Fig. 5(c).

Further, for $k_1 = 0.00169$, the model system (2) again enters into oscillatory fluctuations via subcritical Hopf bifurcation, Fig. 6(a). This figure depicts that for $R_0 \in (0.9814, 0.9857)$, around a stable focus an unstable limit cycle appears. Further, when $R_0 \in (0.9857, 0.9886)$, this stable focus covers itself with two limit cycles (one stable and one unstable) and these two limit cycles collide and annihilates each other at $R_0 \approx 0.9886$. We also generate the phase portrait in $S - I - V$ space for $R_0 = 0.983 \in (0.9814, 0.9857)$ and $R_0 = 0.0987 \in (0.9857, 0.9886)$ in Figs. 6(b) and 6(c), respectively to understand this complex dynamical behavior. From Fig. 6(b), it is clear that as $t \to \infty$, solution trajectories either approach to disease-free equilibrium or stable endemic equilibrium.

For $k_1 = 0.00186$, the model system (2) enters into subcritical Hopf bifurcation at $R_0 = 0.9624$ and the stable endemic equilibrium covers itself with an unstable limit cycle. The generated unstable limit

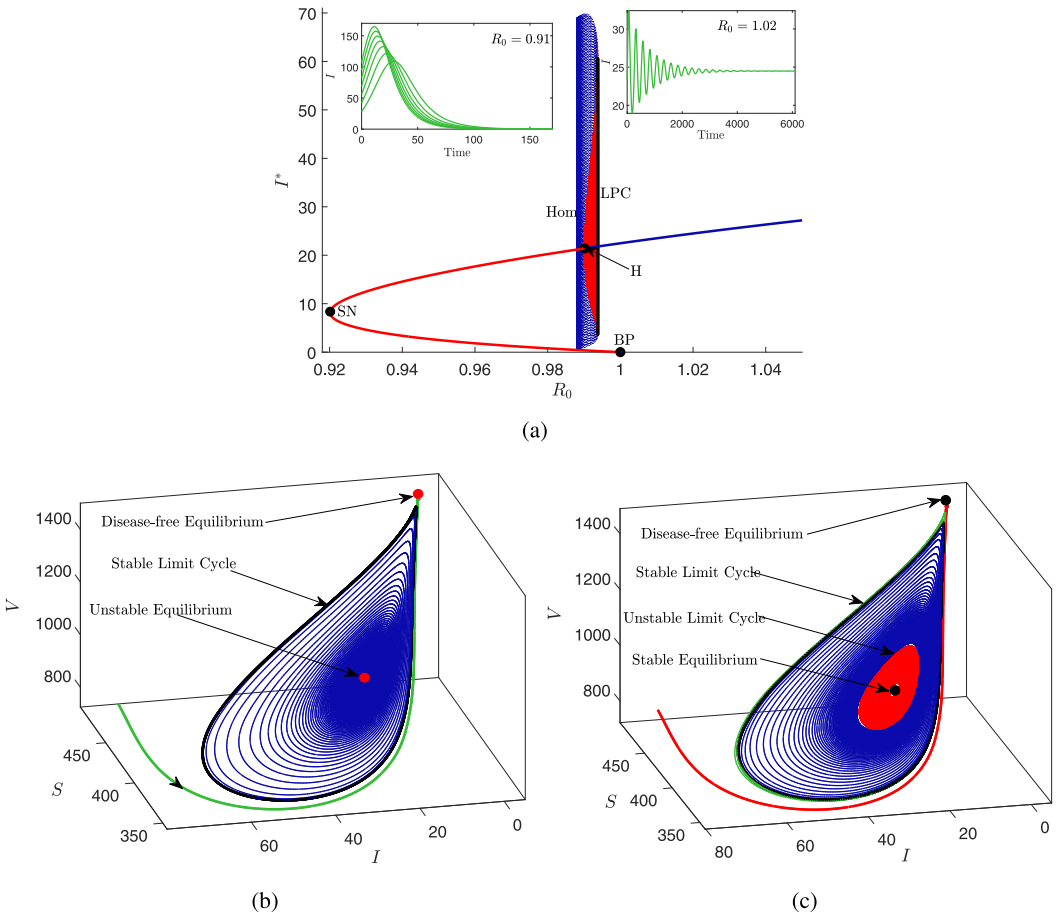

Fig. 5. (a) Bifurcation plot in $R_0 - I^*$ plane for $k_1 = 0.0016$ (b) Phase portrait in $S-I-V$ space for $k_1 = 0.0016$ and $R_0 = 0.989$ (c) Phase portrait in $S-I-V$ space for $k_1 = 0.0016$ and $R_0 = 0.991$.

cycle ceases to appear through homoclinic bifurcation at $R_0 \approx 0.9775$, Fig. 7(a). In this case, the solution trajectories either approach to stable focus or disease-free equilibrium. The phase portrait in $S-I-V$ space for $R_0 = 0.965$ is shown in Fig. 7(b).

Further, when we plot equilibrium curve in $R_0 - I$ plane for $\beta_1 = 0.0058$, $\nu_1 = 0.39$, $\alpha = 0.065$, $k_1 = 0.02296$, $H_a = 418$ and $\phi_0 = 0.09$, it is observed that the equilibrium curve comprises of two SN points (at $R_0 \approx 0.0.93$ and $R_0 \approx 1.0105$) and two Hopf points H_1 (at $R_0 \approx 1.043$) and H_2 (at $R_0 \approx 1.0056$), Fig. 8. The existence of two saddle–node points indicates that the equilibrium curve displays three distinct branches. Consequently, the system exhibits three endemic equilibria for $R_0 \in (1, 1.0105)$. Also, the presence of Hopf points results in the destabilization of all three branches of the equilibrium curve. Moreover, the Hopf point H_1 is of subcritical in nature, resulting in the stable endemic equilibrium being surrounded by two limit cycles. Among these, the inner limit cycle is unstable, while the outer one is stable. A collision between these two limit cycles occurs, followed by their disappearance through a limit cycle bifurcation at approximately $R_0 \approx 1.045$. The stable limit cycle further experiences a homoclinic bifurcation at $R_0 \approx 1.00158$. Furthermore, Hopf point H_2 exhibits a supercritical nature. This means that an unstable endemic equilibrium is encircled by a stable limit cycle, which, in turn, is covered by an unstable limit cycle. These two limit cycles undergo a limit cycle bifurcation at approximately $R_0 \approx 1.002$, and the unstable limit cycle experiences a homoclinic bifurcation at $R_0 \approx 1.0015$.

(d) *Bogdanov–Takens bifurcation:*

To show appearance of BT bifurcation of co-dimension 2, we choose R_0 and k_1 as bifurcation parameters. In Fig. 9(a), homoclinic (Hom), saddle–node (SN), and Hopf (H) curves join at the 'BT' point and dispart the $R_0 - k_1$ plane into four regions. In these regions, system (2) exhibits four different dynamical behaviors.

(i) At BT point (R_0, k_1), the proposed model system (2) has a saddle endemic equilibrium and a disease-free equilibrium. In this case, all the solution trajectories approach to disease-free equilibrium, Fig. 9(b).

(ii) For the values of R_0 and k_1 from Region I, model system (2) has only disease-free equilibrium. Therefore, solution trajectories move towards disease-free equilibrium irrespective of their initial start. The phase portrait in $S-I-H$ space for $(R_0, k_1) \approx (0.974, 0.0012) \in$ Region I is shown in Fig. 9(c).

(iii) The model system (2) exhibits two endemic equilibrium and both are saddle in nature for the value of R_0 and k_1 from Region II. In this case also, all the solution trajectories approach towards disease-free equilibrium. The phase portrait in $S-I-H$ space for $(R_0, k_1) \approx (0.979, 0.0012) \in$ Region II is represented in Fig. 9(d).

(iv) In Region III, model system (2) exhibits two saddle endemic equilibria. Saddle equilibrium with high endemicity surrounds itself with a stable limit cycle and hence all the solution trajectories either spiral towards stable limit cycle or approach to disease-free equilibrium. The phase portrait in $S-I-H$ space for $(R_0, k_1) \approx (0.979, 0.00121) \in$ Region III is shown in Fig. 9(e).

(v) For the values of R_0 and k_1 belonging to Region IV, model system (2) has a saddle and a non-saddle endemic equilibrium. Thus, the solution trajectories either move towards disease-free equilibrium or stable endemic equilibrium. The phase portrait in $S-I-H$ space for $(R_0, k_1) \approx (0.975, 0.00123) \in$ Region IV is shown in Fig. 9(f).

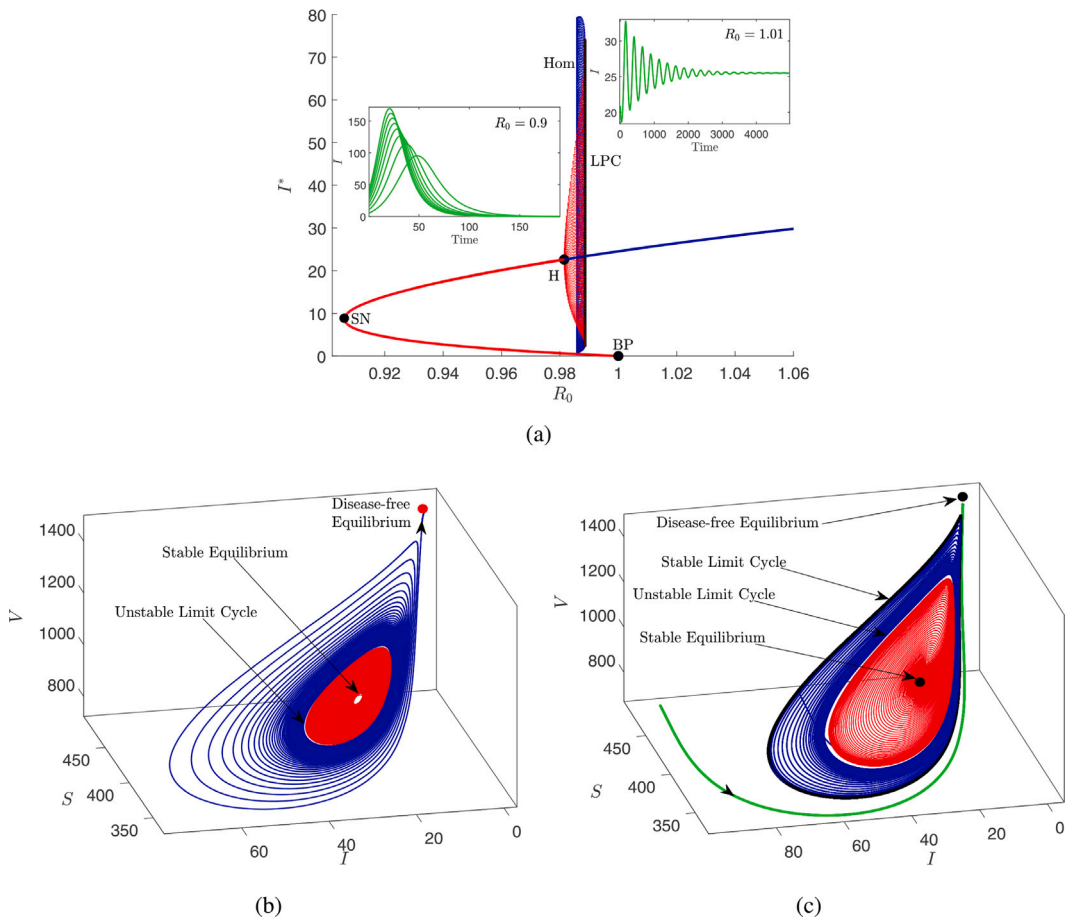

Fig. 6. (a) Bifurcation plot in $R_0 - I^*$ plane for $k_1 = 0.00169$ (b) Phase portrait in $S - I - V$ space for $k_1 = 0.00169$ and $R_0 = 0.983$ (c) Phase portrait in $S - I - V$ space for $k_1 = 0.00169$ and $R_0 = 0.987$.

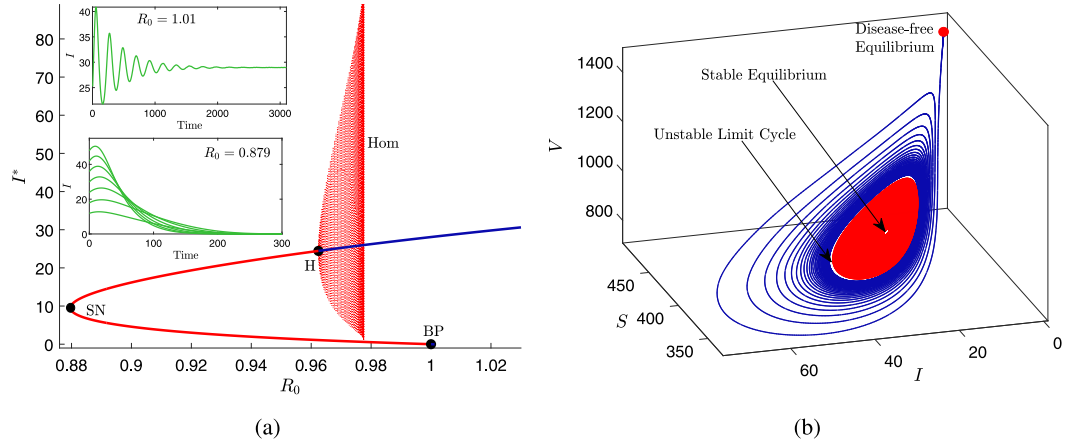

Fig. 7. (a) Bifurcation plot in $R_0 - I^*$ plane for $k_1 = 0.00186$ (b) Phase portrait in $S - I - V$ space for $k_1 = 0.00186$ and $R_0 = 0.965$.

(e) *Generalized Hopf bifurcation:* We choose $k_1 = 0.0013$ and $\sigma = 0.05$ to show the occurrence of generalized Hopf bifurcation. The curve in $\beta - \alpha$ plane comprises two points (GH and BT) and three curves (blue, green and red), Fig. 10(a). Model system (2) exhibits subcritical Hopf bifurcation at red curve and supercritical Hopf bifurcation at green curve. At the blue curve, system (2) undergoes saddle–node bifurcation. The homoclinic orbit at BT point in $S - I - H$ space is shown in Fig. 10(b). The purple point below the red curve in Fig. 10(a) is the point, we choose to plot the phase portrait in Fig. 10(c). Fig. 10(c) shows that two limit cycles bifurcate from the stable focus. The trajectory (red curve) spiral inward to the stable focus and the trajectories (green and blue curves) spiral toward stable limit cycle.

5.2. Impact of vaccination and healthcare facilities

To recognize the impact of hospital beds and vaccination on the infectious disease prevalence, we have plotted variation in the value of R_0 by varying hospitalization rate coefficient k_1 and vaccination rate σ, Fig. 11. Here, it can be easily noted that for small values of

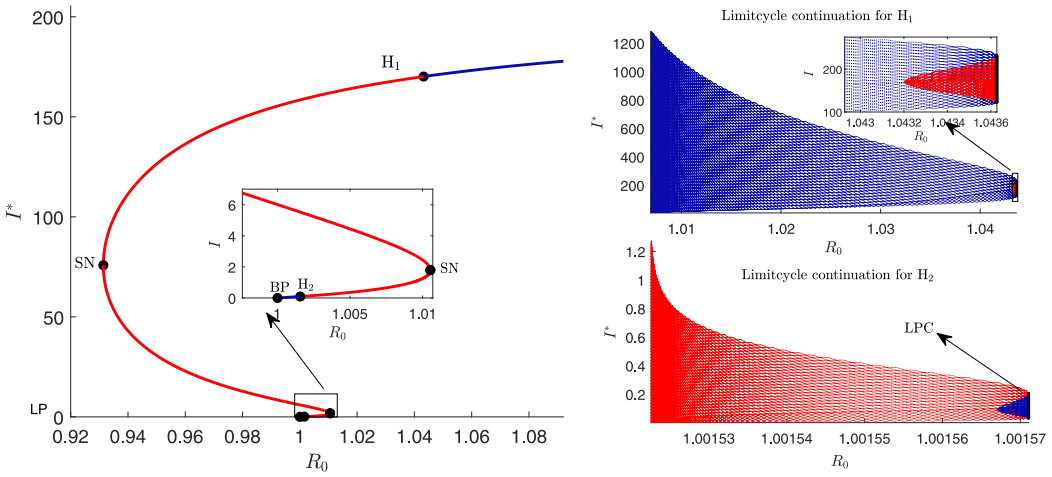

Fig. 8. Bifurcation plot in $R_0 - I$ plane for $\beta_1 = 0.0058$, $\nu_1 = 0.39$, $\alpha = 0.065$, $k_1 = 0.02296$, $H_a = 418$ and $\phi_0 = 0.09$.

k_1 and σ, value of R_0 is higher, whereas on increasing the value of k_1 and σ, value of R_0 decreases. This figure depicts that for the higher values of these parameters, R_0 becomes less than unity, which may ceases the feasibility of endemic equilibrium. Thus, from this figure, it is possible to obtain the required values of k_1 and σ in order to achieve a disease-free equilibrium.

Further, we generate the bar diagram for percentage of equilibrium level of infected individuals, hospitalized individuals, vaccinated individuals and disease-related deaths for 50%, 60%, 70%, 80% and 90% effectiveness of the vaccine, Fig. 12. To generate this bar plot, we choose $\beta = 0.0013$ and $k_1 = 0.00006$. This figure depicts that as the effectiveness of vaccine increases, the percentage of individuals in the infected class decreases. The vaccine with high effectiveness also reduces the surge of patients in hospitals and disease-related deaths. As we increase the effectiveness of vaccine from 50% to 90%, the percentage of individuals in the infected class and disease-related deaths decrease by 8.09% and 1.619%, respectively

In Fig. 13, we have made graphs by varying hospital bed increment rate (ϕ) and vaccination rate (σ) for a fixed equilibrium number of infected individuals. In this figure, each curve provides different combinations of ϕ and σ, which will determinate a particular number of infected individuals for the chosen set of parameter values. From this figure, we can obtain the possible set of values for ϕ and σ to maintain a particular level of infected individuals' equilibrium value.

Moreover, we have generated the bifurcation plot in $\phi - I^*$ plane, Fig. 14. From Fig. 14(a), we observe that if we start increasing the parameter ϕ, the equilibrium level of infected individuals starts decreasing till $\phi = 0.02671$. Further, the system enters into stable limit cycle oscillations via supercritical Hopf bifurcation, and these oscillations ceases to appear at $\phi = 0.06395$. Between these two points, the number of infected individuals fluctuates depending upon the amplitude of the stable limit cycle. Afterwards, the equilibrium level of infected individuals eventually declines to zero. In Fig. 14(b), the system enters into limit cycle oscillation via subcritical Hopf bifurcation at $\phi = 0.01517$ (marked with H_1). In the left side of H_1, the stable equilibrium covers up itself with two limit cycles (inner one is unstable and outer one is stable). These two limit cycles collide and cease to appear limit cycle bifurcation at $\phi = 0.01502$. Thus, $\phi \in (0.01502, 0.01517)$, all the solution trajectories approach to either stable equilibrium or stable limit cycle. Further, in the right side of point H_1, stable focus becomes unstable and covers itself with stable limit cycle and the limit cycle ceases to appear via supercritical Hopf bifurcation at $\phi = 0.05769$. Thus, $\phi \in (0.01517, 0.05769)$, all the solution trajectories approach stable limit cycle. This implies that, the number of infected individuals fluctuates depending on the amplitude of the limit cycle.

6. Conclusion

In epidemiology, healthcare facilities (more precisely number of hospital beds) and vaccines are cornerstones in the management of infectious diseases outbreak and the surest mean to decline the epidemic risk. In the present work, we have proposed and studied a mathematical model to stimulate the impact of healthcare facilities in terms of number of hospital beds with vaccination. We considered that with the increase in infected population, the number of beds in hospitals is also increased. We have provided a detailed study regarding the stability of endemic and disease-free equilibria and the possibility of the existence of different kinds of bifurcations. The proposed model system can have two endemic equilibria when the basic reproductive number is below unity. The dynamical properties of the proposed model system include the co-existence of two limit cycles, bi-stability (disease-free equilibrium and endemic equilibrium or endemic equilibrium and limit cycle) and tri-stability (disease-free equilibrium, endemic equilibrium, and limit cycle).

Using the center manifold theorem for transcritical bifurcation, we obtained a threshold quantity for hospitalization rate coefficient. The direction of transcritical bifurcation is forward when the hospitalization rate coefficient is lower than the threshold quantity, which implies the disease can be rooted out if the basic reproduction number is less than 1, and persists if greater than 1. For hospitalization rate coefficient above the threshold value, the disease-free zone can be increased, but at the same time, the surge of patients in hospitals may take place, which causes a complex situation through backward bifurcation. The development of policies to diminish the prevalence of an infectious disease will require some additional precautions in this scenario. Since a stable endemic equilibrium co-exists with the disease-free equilibrium; thus, the basic reproduction number below unity is a sufficient condition to root out the disease from the population only when the number of infected individuals is small enough.

Further increase in hospitalization rate coefficient, large-amplitude oscillations are observed in our model, which provide a more reasonable explanation for disease recurrence. Through the numerical simulations, we have shown that the system is stable for the small values of disease transmission rate (or equivalently basic reproduction

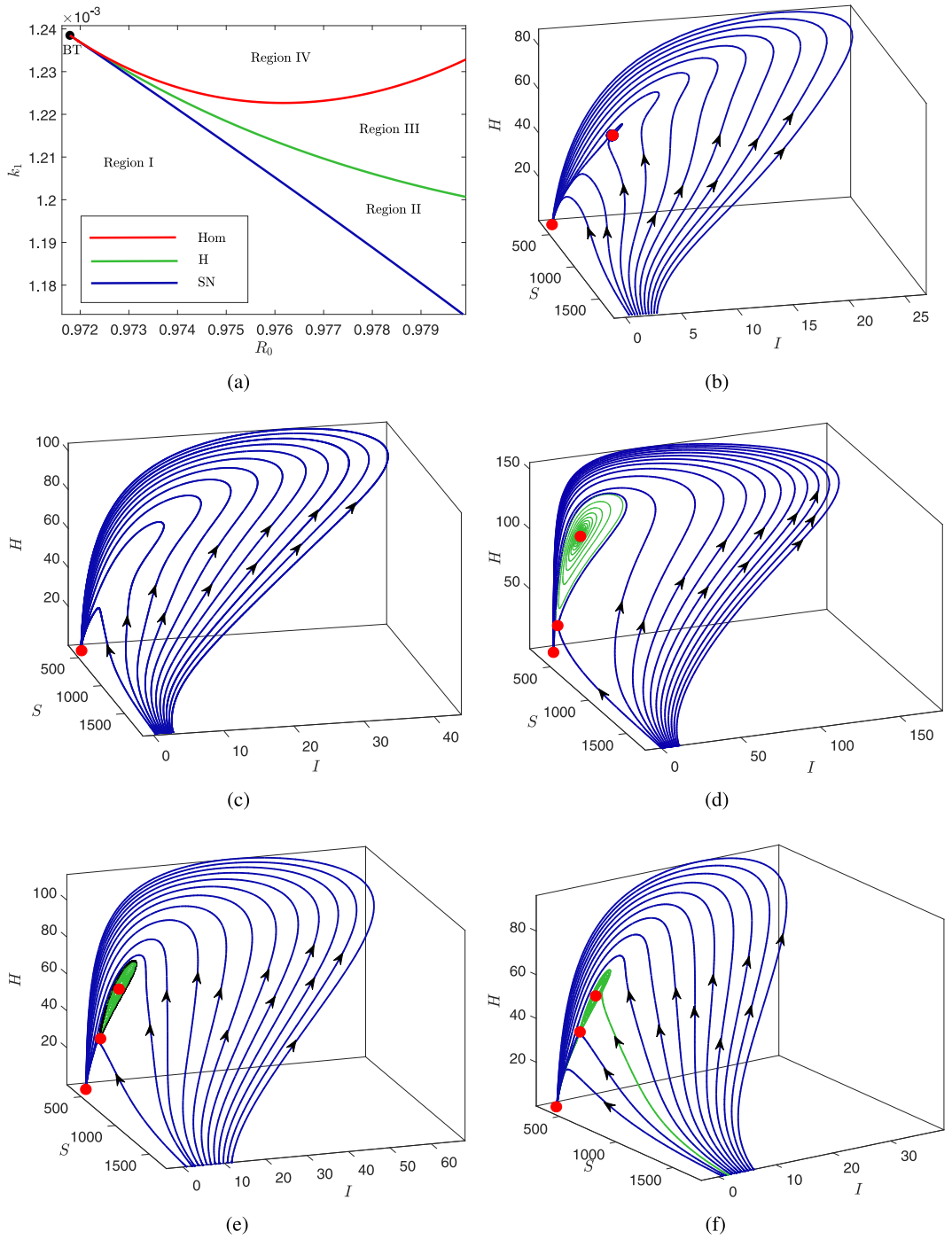

Fig. 9. (a) Bifurcation plot in $R_0 - k_1$ plane for $\phi = 0.05$. Phase portrait in $S - I - H$ space for (b) $R_0 = 0.9718$, $k_1 = 0.00124$ (BT point) (c) $R_0 = 0.974$, $k_1 = 0.0012$ (Region I) (d) $R_0 = 0.979$, $k_1 = 0.0012$ (Region II) (e) $R_0 = 0.979$, $k_1 = 0.00121$ (Region III) (f) $R_0 = 0.975$, $k_1 = 0.00123$ (Region IV).

number) and enters into limit cycle oscillations after a certain threshold. Thus, on increasing the value of disease transmission rate, the number of infected individuals fluctuates in a range depending on the amplitude of the limit cycle. Since the number of infected individuals oscillates continuously, healthcare managers and policy-makers will have difficulties in making strategies to diminish the prevalence of infectious disease. Further, it is shown that the proposed system experiences saddle–node bifurcation with respect to the disease transmission rate as well as BT bifurcation of co-dimension 2. The scenario of BT bifurcation depicts that, for the nearby parameter values of 'BT" point, the formulated system exhibits two limit cycles, which is not requisite from the public health standpoint.

The simulation of the proposed model depicts interesting results. We found that for the higher rate of vaccination and hospitalization, basic reproduction number becomes less than unity, which ceases the existence of endemic equilibrium. Also, by increasing vaccine effectiveness

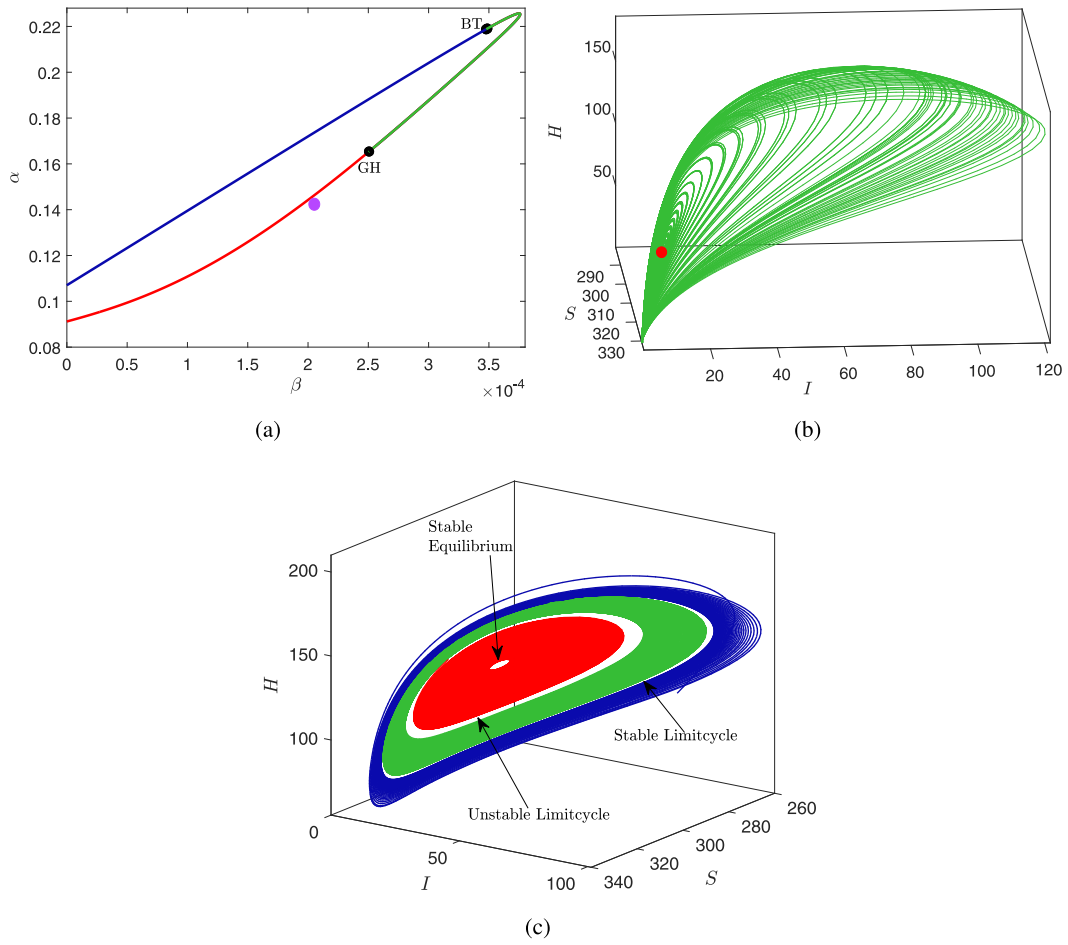

Fig. 10. (a) Bifurcation plot in $\beta - \alpha$ plane for $k_1 = 0.0013$, and $\sigma = 0.05$ (b) Homoclinic curve in $S - I - H$ space (c) Phase portrait in $S - I - H$ space for $\beta = 0.0002075$ and $\alpha = 0.141$.

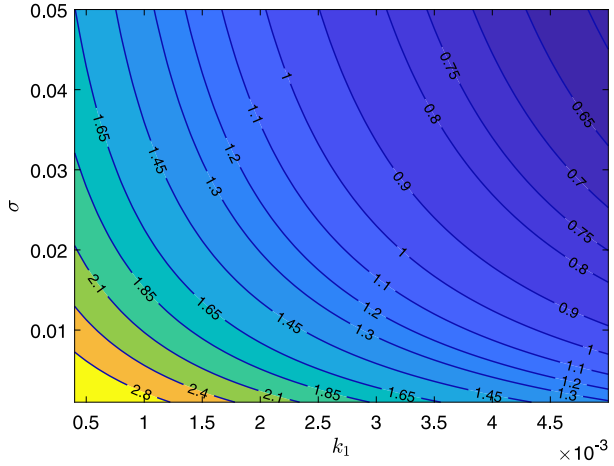

Fig. 11. Effect of changing values of k_1 and σ on R_0. All the parameter values are same as in Table 3 except $\beta = 0.0005$.

from 50% to 90%, we can reduce the number of infected individuals as well as mobs in hospitals. Also, based on the numerical results, for the selected set of parameter values, it is possible to calculate the required values of increment rate of hospital beds and vaccination rate to maintain a particular number of infected individuals.

Our study shows that the disease transmission dynamics depends on more than just the basic reproduction number. The dynamics of disease transmission is also greatly influenced by other epidemiological parameters (such as hospital beds and vaccines). Moreover, the outcomes of our study might be helpful to public health authorities

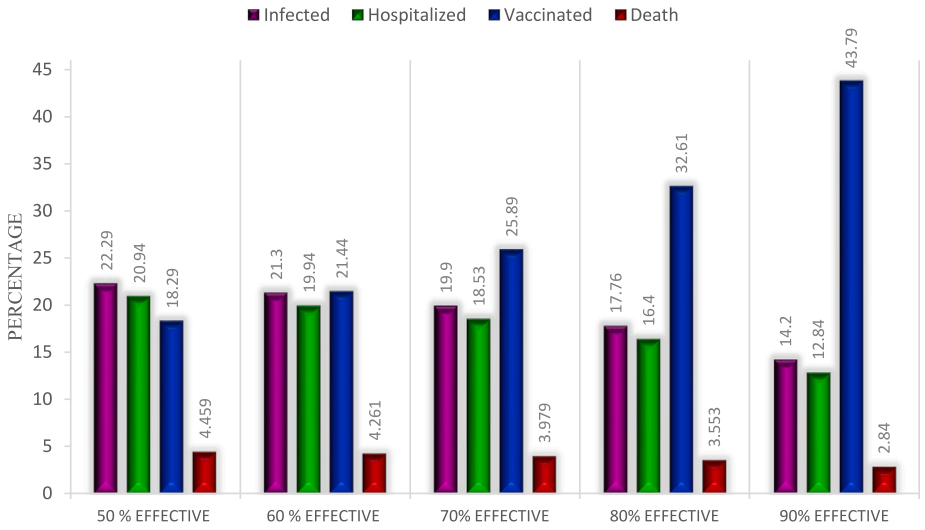

Fig. 12. Bar graph showing the change in percentage of infected individuals (magenta), hospitalized individuals (green), vaccinated individuals (blue) and disease-related deaths (red) with the change in effectiveness of vaccine. All the parameter values are same except $\beta = 0.0013$ and $k_1 = 0.00006$.

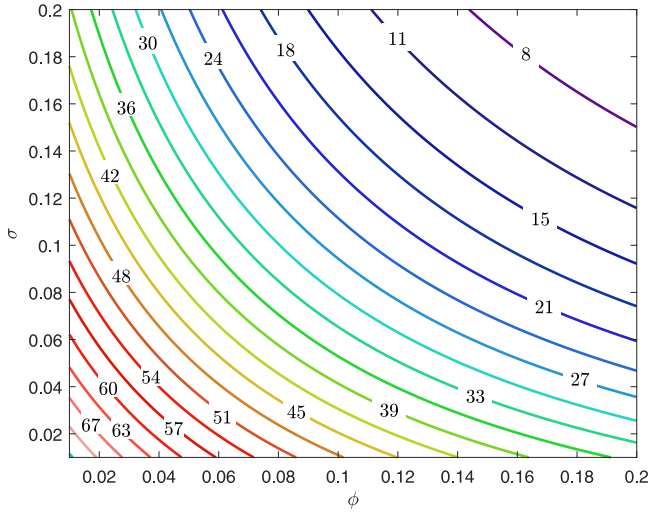

Fig. 13. Effect of changing values of ϕ and σ on the number infected individuals. All the parameter values are same except $\beta = 0.0016$ and $k_1 = 0.0013$.

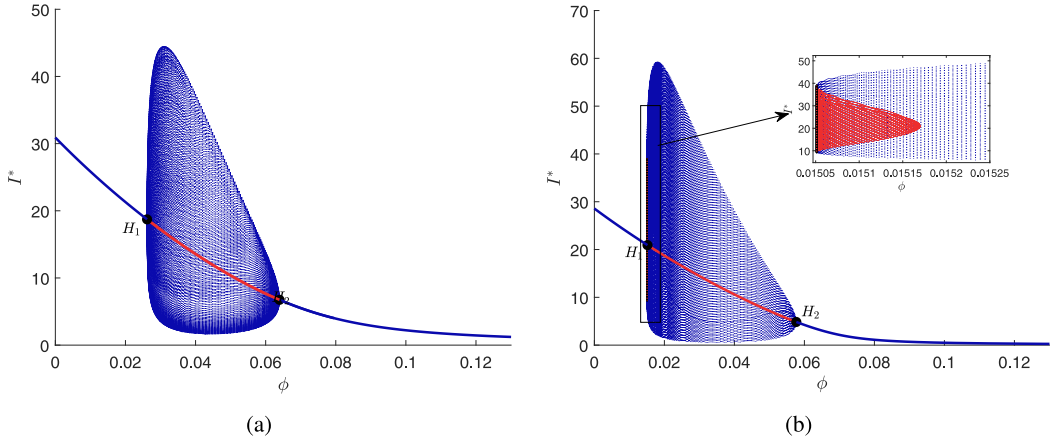

Fig. 14. Bifurcation plot in $\phi - I^*$ plane for (a) $\beta = 0.000267$, $d = 0.01$, and $\sigma = 0.027$, (b) $\beta = 0.000267$, $d = 0.01$, and $\sigma = 0.033$.

in developing their plans for allocating resources in order to diminish infectious disease transmission in the future.

Declaration of competing interest

We confirm that this paper has been read and approved by all the authors and that there are no other persons who satisfied the criteria for authorship but are not listed. We further confirmed that the order of authors listed in this paper has been approved by all of us.

Acknowledgment

Authors are thankful to anonymous reviewers for their fruitful suggestions, which have improved the earlier draft of this paper. A. K. Misra also thankfully acknowledge the financial support from DST-Science and Engineering Research Board, MATRICS Expert committee (File No. MTR/2021/000819) to carry out this research work.

References

[1] Death by age, Available at https://ourworldindata.org/grapher/daly-rates-from-all-causes-by-age.
[2] Our World Bank in Data, death rate, per 10 00, 000 people, available at https://ourworldindata.org/grapher/infectious-disease-death-rates?tab=table.
[3] World health statistic, available at https://apps.who.int/iris/bitstream/handle/10665/81965/9789241564588_eng.pdf?sequence=1.
[4] The World Bank, Hospital beds population ratio available at https://data.worldbank.org/indicator/SH.MED.BEDS.ZS?most_recent_year_desc=true.
[5] R.E. Baker, A.S. Mahmud, I.F. Miller, M. Rajeev, F. Rasambainarivo, B.L. Rice, S. Takahashi, A.J. Tatem, C.E. Wagner, L.F. Wang, A. Wesolowski, C.J.F. Metcalf, Infectious disease in an era of global change, Nat. Rev. Microbiol. 20 (4) (2022) 193–205.
[6] A. Abdelrazec, J. Belair, C. Shan, H. Zhu, Modeling the spread and control of dengue with limited public health resources, Math. Biosci. 271 (2016) 136–145.
[7] M.A. Acuna-Zegarra, S. Diaz-Infante, D. Baca-Carrasco, D. Olmos-Liceaga, COVID-19 optimal vaccination policies: A modeling study on efficacy, natural and vaccine-induced immunity responses, Math. Biosci. 337 (2021) 108614.
[8] S.D. Djiomba Njankou, F. Nyabadza, Modelling the potential impact of limited hospital beds on Ebola virus disease dynamics, Math. Methods Appl. Sci. 41 (2018) 8528–8544.
[9] I. Dorigatti, A. Pugliese, Analysis of a vaccine model with cross-immunity: when can two competing infectious strains coexist? Math. Biosci. 234 (1) (2011) 33–46.
[10] J. Kopfova, P. Nabelkova, D. Rachinskii, S.C. Rouf, Dynamics of SIR model with vaccination and heterogeneous behavioral response of individuals modeled by the Preisach operator, J. Math. Biol. 83 (2) (2021) 1–34.
[11] C. Kribs-Zaleta, J. Velasco-Hernandez, A simple vaccination model with multiple endemic states, Math. Biosci. 164 (2000) 183–201.
[12] X. Liu, Y. Takeuchi, S. Iwami, SVIR epidemic models with vaccination strategies, J. Theoret. Biol. 253 (1) (2008) 1–11.
[13] J. Mohammed-Awel, E. Numfor, R. Zhao, S. Lenhart, A new mathematical model studying imperfect vaccination: Optimal control analysis, J. Math. Anal. App. 500 (2) (2021) 125132.
[14] J. Mushanyu, F. Nyabadza, G. Muchatibaya, P. Mafuta, G. Nhawu, Assessing the potential impact of limited public health resources on the spread and control of typhoid, J. Math. Biol. 77 (3) (2018) 647–670.
[15] A.K. Misra, J. Maurya, Modeling the importance of temporary hospital beds on the dynamics of emerged infectious disease, Chaos 31 (10) (2021) 103125.
[16] A.K. Misra, J. Maurya, M. Sajid, Modeling the effect of time delay in the increment of number of hospital beds to control an infectious disease, Math. Biosci. Eng. 19 (11) (2022) 11628–11656.
[17] A.K. Misra, J. Maurya, Bifurcation analysis and optimal control of an epidemic model with limited number of hospital beds, Int. J. Biomath. (2022) 2250101, http://dx.doi.org/10.1142/S1793524522501017.
[18] J.F. Oliveira, D.C.P. Jorge, R.V. Veiga, M.S. Rodrigues, M.F. Torquato, N.B. da, Silva, R.L. Fiaccone, L.L. Cardim, F.A.C. Pereira, C.P. de Castro, A.S.S. Paiva, A.A.S. Amad, E.A.B.F. Lima, D.S. Souza, S.T.R. Pinho, P.I.P. Ramos, R.F.S. Andrade, Mathematical modeling of COVID-19 in 14.8 million individuals in Bahia, Brazil, Nature Commun. 12 (1) (2021) 1–13.
[19] F. Rao, P.S. Mandal, Y. Kang, Complicated endemics of an SIRS model with a generalized incidence under preventive vaccination and treatment controls, Appl. Math. Model. 67 (2019) 38–61.
[20] V. Rao, R.K. Upadhyay, Modeling the spread and outbreak dynamics of avian influenza (H5N1) virus and its possible control, Dyn. Models Infect. Dis. (2013) 227–250, http://dx.doi.org/10.1007/978-1-4614-9224-5_9.
[21] C. Shan, H. Zhu, Bifurcations and complex dynamics of an SIR model with the impact of the number of hospital beds, J. Differ. Equ. 257 (2014) 1662–1688.
[22] C. Shan, Y. Yi, H. Zhu, Nilpotent singularities and dynamics in an SIR type of compartmental model with hospital resources, J. Differ. Equ. 260 (5) (2016) 4339–4365.
[23] N. Stollenwerk, C.D.S. Estadilla, J. Mar, J.B. Van-Dierdonck, O. Ibarrondo, R. Blasco-Aguado, M. Aguiar, The effect of mixed vaccination rollout strategy: A modelling study, Infect. Dis. Model. 8 (2) (2023) 318–340.
[24] H. Wei, Y. Jiang, X. Song, G.H. Su, S.Z. Qiu, Global attractivity and permanence of a SVEIR epidemic model with pulse vaccination and time delay, J. Comput. Appl. Math. 229 (1) (2009) 302–312.
[25] L. Zhou, M. Fan, Dynamics of an SIR epidemic model with limited medical resources revisited, Nonlinear Anal. RWA 13 (1) (2012) 312–324.
[26] J. Arino, E. Milliken, Bistability in deterministic and stochastic SLIAR-type models with imperfect and waning vaccine protection, J. Math. Biol. 84 (7) (2022) 61.
[27] P. Van den Driessche, J. Watmough, Reproduction numbers and sub-threshold endemic equilibria for compartmental models of disease transmission, Math. Biosci. 180 (2002) 29–48.
[28] C. Castillo-Chavez, B. Song, Dynamical models of tuberculosis and their applications, Math. Biosci. Eng. 1 (2) (2004) 361.
[29] L. Perko, Differential Equations and Dynamical Systems, Vol. 7, Springer Science & Business Media, 2013.